



Internship report

**Finite Element Stress Analysis and Structural Assessment in an
Engineering Consultancy Internship**

Delphine FOUQUET

Academic year 2020-2021

MOCA Second year

3rd May 2021 - 24th July 2021

Internship tutors : Dr. Angus RAMSAY, Mrs. Lyudmyla YUSHCHENKO

Table of contents

Engagement de non plagiat	1
Abstract	2
Acknowledgments	2
1 Introduction	2
2 Problem of a lamp column	3
2.1 Hand calculation of M_y and M_p	4
2.2 First modelisation with ANSYS	5
2.3 Study on the beam element in ANSYS	7
3 Problem of a plate with a hole	9
3.1 Mesh convergence for average stresses using ANSYS	10
3.2 Stress concentration factor K	12
3.3 Improvement of the mesh	16
4 Introduction to the Lamé equations on a cylinder	18
4.1 First use of the LFE software	19
4.2 Mesh convergence study	21
4.3 Thick-walled internally pressurised cylinder	23
4.3.1 Design chart	23
4.3.2 Comparison of three yield criteria	27
5 Rotors	32
5.1 Rotating annular disk	32
5.2 Three-part rotor only subjected to centrifugal loading	34
5.3 Three-part rotor subjected to centrifugal loading and surface forces	36
5.4 Annular disk assembled on a solid shaft with a shrink-fit	39
5.5 Constant thickness disk with radial slots	41

6 Commercial project	44
6.1 Simply Supported Rectangular Plate under UDL	44
6.1.1 Theoretical solution	44
6.1.2 Simulation with ANSYS	45
6.1.3 Closure	46
6.2 Balustrade	47
6.2.1 Model of the balustrade	47
6.2.2 Modelling with ANSYS	47
6.2.3 Boundary conditions	48
7 Conclusion	49
References	50

Table of figures

1	X-component of stress for a load of 1 kNm	6
2	Percentage error for different "h" and "p" parameters	8
3	Boundary conditions applied to a quarter plate	10
4	Graphs of the percentage error as a function of the number of elements per edge . . .	11
5	Stress concentration factor K as a function of the number of elements per edge . . .	12
6	Graph comparing the simulated and theoretical K factors, as a function of the d/H ratio	13
7	Percentage error of K depending on the length/width ratio	14
8	Graph comparing the simulated and theoretical K factors, for three different L/H ratios	15
9	Comparison of two meshes : simple on the left and improved on the right	16
10	Graph comparing the simulated and theoretical K factors, with an improved mesh .	17
11	Percentage error made in calculating the K factor with the theoretical solution, for a plate with a hole	18
12	Radial and hoop stresses against the radius for pressurised thick cylinder, LC1 . . .	20
13	Radial and hoop stresses against the radius for pressurised thick cylinder, LC2 . . .	20
14	Convergence of elastic stress for LC2	21
15	Convergence of plastic load factor for LC2 (von Mises criterion)	22
16	Comparison of stresses in thin-walled and thick-walled cylinders, [3]	23
17	Comparison between thick-walled and thin-walled cylinder theory, [3]	24
18	Design chart for internally pressurised pipes	25
19	Tresca curves for L greater than 0.4	27
20	Three yield criteria on the same graph	28
21	Evolution of the normalised stresses as a function of the R ratio for the Tresca criterion	29
22	Comparison of the results obtained with ANSYS and the LFE software	30
23	Maximum percentage strain in the cylinder	31
24	Distribution curves of dimensionless stresses $\sigma_{t,max}/\sigma_0$ and $\sigma_{t,min}/\sigma_0$ as a function of β^2 , for $\nu = 0.3$	33

25	Distribution curves of dimensionless stresses $\tilde{\sigma}_r$ and $\tilde{\sigma}_t$ versus dimensionless radius, for different values of β	34
26	Distribution curves of stresses σ_r and σ_t versus dimensionless radius in the rotor . .	35
27	Radial force and displacement along the radius in the rotor	36
28	Distribution curves of stresses σ_r and σ_t versus dimensionless radius in the rotor . .	37
29	Mesh convergence study for the example of a rotor only subjected to centrifugal loading	38
30	Distribution curves of stresses σ_r and σ_t simulated with ANSYS	38
31	Distribution curves of stresses σ_r and σ_t versus dimensionless radius for different thicknesses h	39
32	Different stresses ($\sigma_t, \sigma_{t,\omega}$ and $\sigma_{t,p}$) versus ω^2 in a shrink-fit shaft/disk assembly . .	40
33	Modeling a disk with radial slots with ANSYS	41
34	Optimised mesh of an angle of a slot	42
35	Comparison of two geometries of an angle of a slot	43
36	Mesh convergence study to show the effect of a singularity	43
37	Percentage error and rate of convergence versus number of elements per edge for three different shell elements in ANSYS	46
38	Maximum transverse deflection of plates with different boundary conditions	49

Engagement de non plagiat

Je soussigné, Delphine FOUQUET
N° carte d'étudiant : 21928957

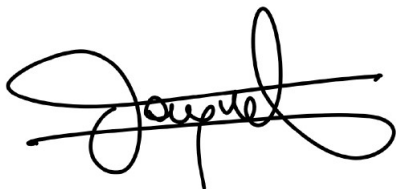
Déclare avoir pris connaissance de la charte des examens et notamment du paragraphe spécifique au plagiat.

Je suis pleinement conscient(e) que la copie intégrale sans citation ni référence de documents ou d'une partie de document publiés sous quelques formes que ce soit (ouvrages, publications, rapports d'étudiants, internet, etc. . . .) est un plagiat et constitue une violation des droits d'auteur ainsi qu'une fraude caractérisée.

En conséquence, je m'engage à citer toutes les sources que j'ai utilisées pour produire et écrire ce document.

Fait le 02/08/2021

Signature(s)

A handwritten signature in black ink, appearing to read 'Delphine Fouquet', with a large, stylized flourish above the name.

Ce document doit être inséré en première page de tous les rapports, dossiers et/ou mémoires.

Document du chapitre 10 annexe 5, issu de la Charte des examens adoptée en Conseil d'Administration le 11 juillet 2013 après avis du CEVU du 27 juin 2013 - Délibération N°2013-73 – Modifié suite au CFVU du 12/03/2015.

Abstract

During my internship at Ramsay Maunder Associates, I completed several projects.

The first one deals with a beam subjected to an end moment. This allowed to see a way to verify ANSYS results, when the theoretical solutions are known. A study on the beam element of the software also allowed to see which element is the best according to the applied load.

The second study is on a plate with a hole. The average stress and the stress concentration factor K were defined, and it was possible to compare the simulated K and the theoretical K . It appeared that the values of K depended on the length over width ratio of the plate and also on the diameter of the hole over width ratio.

The third study introduces the Lamé equations on a thick cylinder. It appeared that, for this model, the ANSYS elements were not that good and that another element, called the Lamé element, could be preferred. A design chart for internally pressurised pipes could then be done using the Lamé element and using three different yield criteria. The difference between those yield criteria was also highlighted.

The fourth study tackles a problem with rotors. In this section, a few examples of a book were reproduced. In doing so, it became apparent that one of the examples in the book was wrong, so it was possible to correct this.

The last study is about a commercial project given by a company that designs balustrades. The model studied was a corrugated plate, it was found that the design given by the company complied with certain European standards. However, the study could not be completed before the internship ended.

Acknowledgments

I would like to thank Dr. Ramsay for being so supportive of my work and for teaching me so much about his profession.

1 Introduction

I completed my second year internship at Ramsay Maunder Associates, a UK-based engineering firm specialising in finite element analysis. My tutor Dr. Angus Ramsay gave me tasks to do and followed me in my work for three months. I did this internship from France, as I could not go to

England because of the Covid-19 pandemic. However, the follow-up was only slightly affected since I had an appointment with my tutor every morning to review my work.

Ramsay Maunder Associates is a small company : there is only one employee, who is Angus Ramsay himself. However, he works with several associates, including Dr. Maunder, who is his former thesis director. Angus Ramsay works daily on several different projects which are mostly sent to him by private companies or law firms. He is also a researcher and has published many articles, he is currently trying to get another one published.

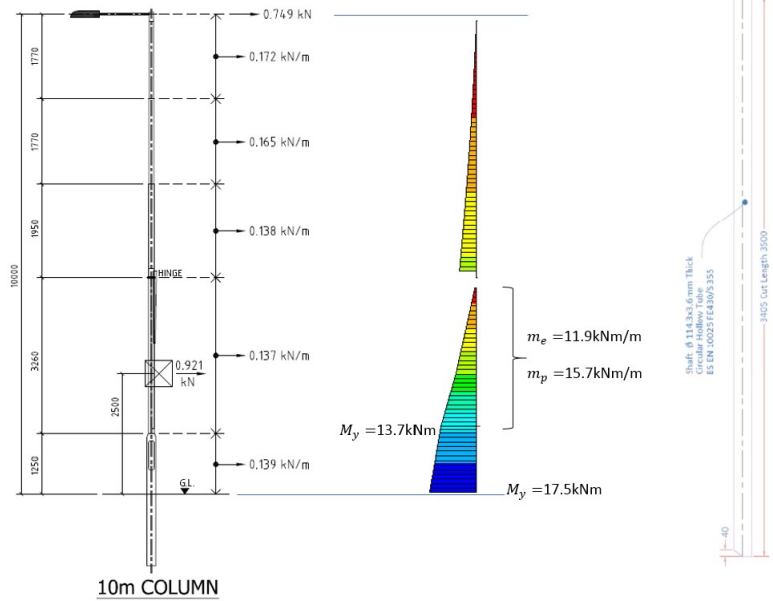
Angus Ramsay works primarily with ANSYS APDL software. I had never used it before, so he asked me a few weeks before my internship to download the software and to familiarize myself with it. At the beginning of the internship, Angus Ramsay suggested that I reproduce a study he was doing for a company, but with a great simplification. This is how we have always proceeded during the entire internship : he gave me projects to do, at first quite simple and then more and more complicated depending on how I progressed and when he saw that I was more and more comfortable with ANSYS. So, there is no predefined subject, it is rather a series of small studies that he gave me to do and that allowed me to learn things.

In the following, a study on a beam subjected to an end moment, a study on a plate with a hole, a study on a thick-walled cylinder, a study on rotors and a commercial project will be seen.

2 Problem of a lamp column

In order to become familiar with ANSYS, a study was first conducted on a simple case to model with the software. In this study, a problem with a beam will be presented and it will be interesting to see how to verify the results provided by the software. In particular, the focus will be on the yield moment M_y and the plastic moment M_p , as the engineers are interested by those data.

The study is about a problem of a lamp column with a hinge, modeled with ANSYS. The details of this and the results are shown below. The results come from a previous study conducted by Angus Ramsay.



To verify the results given by the software, let's first focus on a pipe forming part of the lamp column. It is supposed that the pipe is a beam with a circular hollow section : the inner radius $R_1 = 0.05355\text{m}$ and the outer radius $R_2 = 0.05715\text{m}$. The pipe is made of steel, of yield strength $\sigma_y = 355\text{ MPa}$, of Young's Modulus $E=205\text{ GPa}$ and of Poisson's ratio $\nu = 0.3$. It is important to note that it is a force-driven problem : as the focus will be on stresses and not deflections, the values chosen for E and ν will not influence the results here.

2.1 Hand calculation of M_y and M_p

First of all, let's calculate by hand the elastic and plastic limit moments for the pipe.

Yield Moment M_y

$M_y = S \times \sigma_y$ where σ_y is the yield strength of the material (equal to 355 MPa here) and S is the section modulus as defined below :

$$S = \frac{I}{y} = \pi \frac{(R_2^4 - R_1^4)}{4 \times R_2} = \pi \frac{0.05715^4 - 0.05355^4}{4 \times 0.05715} = 3.3593 \times 10^{-5} \text{ m}^3$$

with y the distance from the neutral axis to the most extreme fibre ($y = R_2$ here).

$$M_y = S \times \sigma_y = 3.3593 \times 10^{-5} \times 355 \times 10^6 = 11.926 \times 10^3 \text{ Nm}$$

$$M_y = 11.926 \text{ kNm}$$

Plastic Moment M_p

$M_p = Z_p \times \sigma_y$ where Z_p is the plastic section modulus defined as followed for a circular hollow section :

$$Z_p = \frac{4(R_2^3 - R_1^3)}{3} = \frac{4(0.05715^3 - 0.05355^3)}{3} = 4.4132 \times 10^{-5} \text{ m}^3$$

$$M_p = Z_p \times \sigma_y = 4.4132 \times 10^{-5} \times 355 \times 10^6 = 15.667 \times 10^3 \text{ Nm}$$

$$M_p = 15.667 \text{ kNm}$$

2.2 First modelisation with ANSYS

Then, let's model this pipe with ANSYS to check whether the results will be the same as those calculated above.

A pipe of one meter along the z axis was modeled and a circular hollow section with the inner radius R_1 and the outer radius R_2 as seen above was defined. A mesh of 8 elements was used, with the default linear shape functions.

A moment of 1 kNm was then applied on one end of the beam, and all degrees of freedom were constrained on the other end. The results obtained are shown in Figure 1 when plotting the X-component of stress. As seen on the graph, the maximum stress is 29.8 MPa. Now, let's divide the yield strength σ_y by this result : a scale factor equal to $\frac{355}{29.8} = 11.9$ is thus obtained. It means that if the load applied is 11.9 times greater than the initial load (1 kNm), the beam will reach the elastic limit $\sigma_y = 355 \text{ MPa}$. This corresponds to the calculated result : it was seen above that the yield moment M_y is equal to 11.926 kNm and it was possible to verify that when a moment of 11.9 kNm is applied on the beam with ANSYS, the maximum stress is equal to 355 MPa.

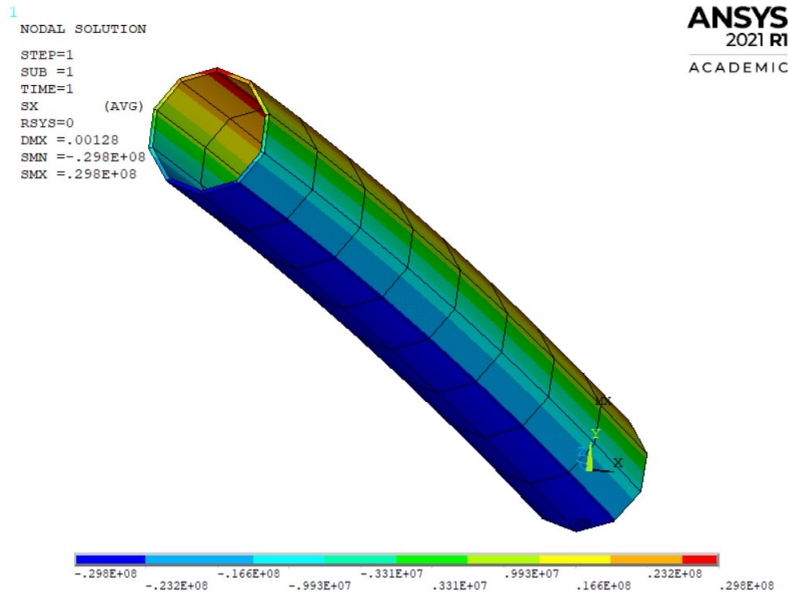


FIGURE 1: X-component of stress for a load of 1 kNm

Now, let's check the results for M_p . According to the calculations, $\frac{M_p}{M_y} = \frac{15.667}{11.926} = 1.314$. It means that the beam can take around 1.3 times more load before reaching plastic limit. If a moment ten-times greater than the previous case is applied on the beam (the moment applied is now 119 kNm), it can be noted that ANSYS will stop the calculations at 0.133 s. After that time, the moment applied has passed the plastic limit M_p and the software is not able to calculate a solution anymore.

At 0.133 s of the simulation, the load applied on the beam is equal to 0.133 times the total load of 119 kNm, so the load applied is $0.133 \times 119 = 15.827 \text{ kNm}$. This value is very close to the plastic moment $M_p = 15.667 \text{ kNm}$ calculated before.

Thanks to that, it is possible to verify the results given by the software.

In this short study, it was seen how to calculate by hand the yield moment and the plastic moment of a beam with a circular hollow section. Furthermore, it was seen how to verify the results given by the software. In any future projects with ANSYS, it should always be remembered to do this code verification to give credibility to the results obtained.

2.3 Study on the beam element in ANSYS

For the previous study with ANSYS, a linear beam element of 8 nodes was used. These parameters were chosen without checking that there was a mesh convergence, as this was a first simulation with ANSYS to get started with it. Now, after several weeks of using the software and having gained some experience, let's carry out a convergence study of the beam element. This was facilitated by the use of the ANSYS APDL code, which allows commands to be automated and thus a large number of simulations to be run by changing a few parameters very quickly and easily.

There are two parameters that can be changed to refine the beam element : the "p" parameter and the "h" parameter. The "p" parameter is the degree of the element, it can be linear, quadratic or cubic. By default, it is the linear shape function that is used in ANSYS. On the other hand, the "h" parameter is the number of elements used in the mesh. In general, the greater the number of elements, the more accurate the solution, but the longer the calculation so compromises have to be made.

To do the study, let's focus on the bending moment of a cantilever beam induced by various forms of applied load, for instance an end moment, an end load, a uniformly distributed load (UDL) and a linearly distributed load (LDL). These cases were chosen because their theoretical results are well known :

- For an end moment M , the bending moment in the beam is equal to the moment applied, the moment distribution will then be constant.
- For an end load W , the bending moment in the beam is equal to $-Wx$ where x is the distance from the free end of the beam. The moment distribution will then vary linearly.
- For a UDL w , the bending moment in the beam is equal to $-\frac{wx^2}{2}$, the moment distribution will then vary quadratically.
- For a LDL, the bending moment in the beam is equal to $-\frac{w_0x^3}{6L}$, where w_0 is the load applied at the fixed end and L is the length of the beam. The moment distribution will then vary cubically.

In ANSYS, the beam is modelled with a length of one metre, a rectangular section of $0.1 \times 0.1\text{m}$, a Young's modulus of 200 GPa, a Poisson's ratio of 0.3 and with the element BEAM188. Two do-loops in ANSYS APDL were used to change the number of elements (parameter "h") and the shape functions of the elements (parameter "p"). All degrees of freedom of one end of the beam were constrained.

For all types of loads, the focus was on the bending moment of the I-node of the first element, which corresponds to the node at the fixed end. This also corresponds to the maximum value of the bending moment of the beam.

When applying an end moment of 10 Nm on the beam, the bending moment was always equal to 10 Nm regardless of the number of elements or their type. This result is consistent with the theory. In the case of an end force, a UDL and a LDL, the result varied according to the number of elements and the type of element. The percentage errors calculated between theoretical and simulated values of bending moments are shown in Figure 2 for the three different loads. The percentage error was obtained with the following formula : $\%error = \frac{M_{theoretical} - M_{simulated}}{M_{theoretical}}$, with M the bending moment.

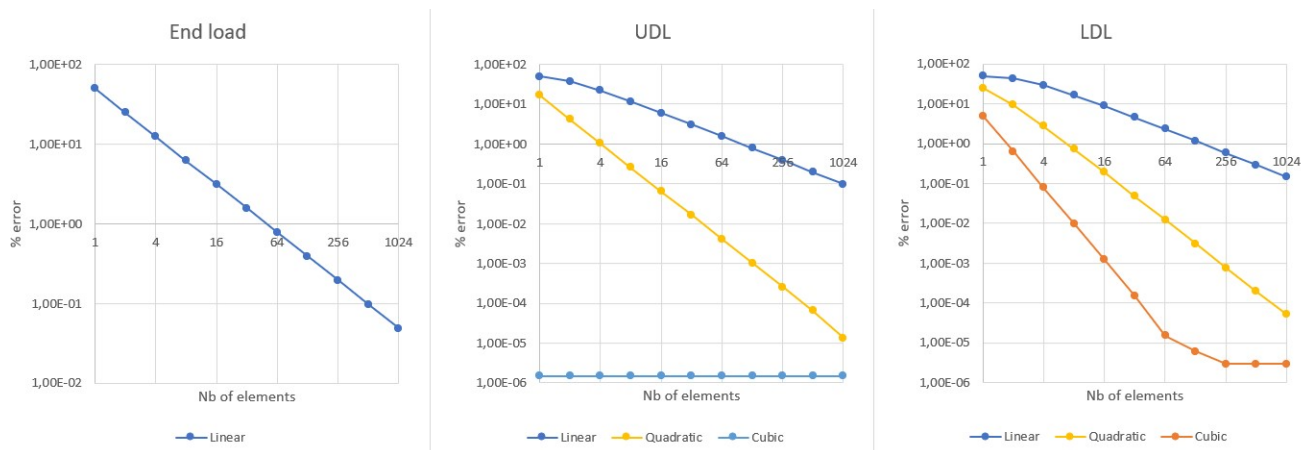


FIGURE 2: Percentage error for different "h" and "p" parameters

In the case of the end load, the quadratic and cubic elements gave the exact solution regardless of the number of elements. This is because for a beam with an end load, the bending moment vary linearly according to the theory : it seems like an element with a degree "p" higher than the degree of the solution will give the exact solution. For the linear element, up to 64 elements are required for the error to be less than 1% which shows a rather poor convergence.

In the case of the UDL (quadratic solution), it is only the cubic elements that give the exact solution regardless of the number of elements (percentage error nearly equal to zero). With quadratic elements, the convergence is linear and quite fast : it takes 4 elements to reach 1% error. However, for the linear elements, a large number of elements are needed to reach the asymptotic region of uniform convergence rate.

Finally, for the case of the LDL (cubic solution), the cubic elements allow a very fast convergence : it takes only two elements to reach 1% error. Quadratic elements are slightly less efficient as they require 8 elements to achieve 1% error, and the worst ones are the linear elements which need more than 128 elements to get to 1% error.

Note : For the UDL case, the cubic element should give an error of 0%. However, as seen on the graph, this is not exactly the case as the error is constant and about equal to $1e-6\%$. Similarly for the LDL case, the cubic element should have a linear convergence, but after a certain number of elements the error stagnates around $1e-6\%$ too. It would seem that the ANSYS cubic element always produces a small error, but the cause of this error has not yet been identified.

In conclusion of this small study, it seems obvious that choosing the type of element according to the applied load is important to have good simulated results, and one should also be careful with the number of elements used. It also seems that whatever the type of load, the linear elements are very poor. As this is the default element type in ANSYS, care must be taken with this while doing a simulation.

3 Problem of a plate with a hole

The following study was conducted to determine the stress concentration factor K in a plate with a hole, as a function of the hole diameter to plate width ratio. For this purpose, it is necessary to conduct a mesh convergence study to choose the number of elements that will ensure the lowest percentage error between theoretical and calculated values.

First of all, let's define the notations of the problem.

Let's consider a plate of length $L=60\text{mm}$, thickness 1m (by default) and width $H=40\text{mm}$. It is pierced in the middle by a hole of diameter $d=10\text{mm}$, and it is made of aluminium with a Young's modulus of 69 GPa and a Poisson's ratio of 0.30 . The plate is pulled on both sides with a force F of 10 MN .

3.1 Mesh convergence for average stresses using ANSYS

The problem is then modelled with ANSYS. As the problem is symmetrical with two planes of symmetry, it is possible to model only a quarter of the plate without changing the results obtained. To do this, symmetric boundary conditions must be applied as shown in Figure 3 : the normal displacement of the left and the bottom edge are blocked but not the tangential displacement.

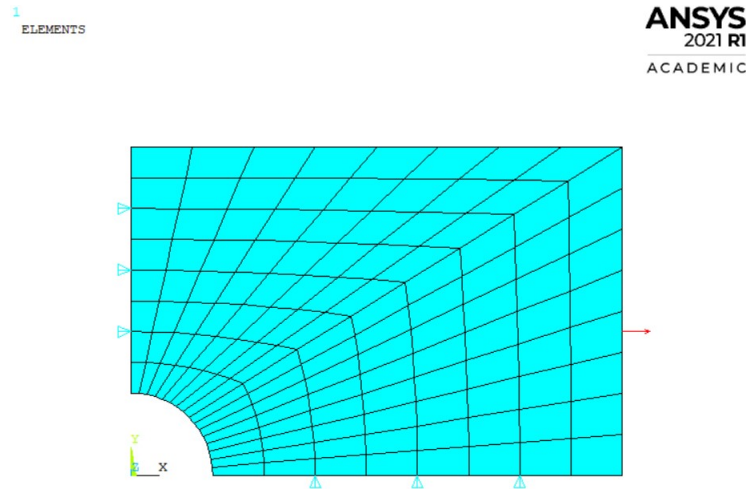


FIGURE 3: Boundary conditions applied to a quarter plate

Instead of applying a force of 10 MN, a pressure of 250 MPa is applied to the right edge of the plate, represented by a red arrow in the figure.

The focus is on the distribution of the stress in the plate. In the case of an axial load that causes tension or compression, the average stress is given by the formula

$$\sigma = \frac{\text{Axial force } F}{\text{Cross section area}}$$

Let's consider the cross section that goes across the hole. The cross section area is then equal to : $\text{area of the plate} - \text{area of the hole} = 0.04 \times 1 - 0.01 \times 1 = 0.03 \text{ m}^2$. That leads to a calculated average stress across the hole $\sigma_{\text{across hole}} = \frac{10 \times 10^6}{0.03} = 333.33 \times 10^6 \text{ Pa}$.

Then, let's consider the cross section of the right edge of the plate, on which the force is applied. The cross section area is equal to 0.04 m^2 . That leads to a calculated average stress on the right

edge of the plate $\sigma_{right\ edge} = \frac{10 \times 10^6}{0.04} = 250 \times 10^6$ Pa.

After running the simulation for 4-node and 8-node elements and for a number of elements per edge ranging from 1 to 128, the average stresses obtained with the software (let's name them $\sigma_{software}$) are used to calculate the percentage error, displayed in the tables and on the graphs in Figure 4. There are two different graphs depending on the cross section chosen : either across the hole or on the right edge of the plate. The results printed are the percentage error, which is calculated as follows : $\%error = \frac{\sigma_{calculated} - \sigma_{software}}{\sigma_{calculated}} \times 100$, where $\sigma_{calculated}$ is equal to $\sigma_{across\ hole}$ or $\sigma_{right\ edge}$ depending on the case.

Across hole								
nb of elements	1	2	4	8	16	32	64	128
% error_hole (4 nodes)	3,97E+00	1,07E+00	6,21E-01	1,41E-01	2,10E-02	8,10E-02	8,10E-02	8,10E-02
% error_hole (8 nodes)	5,75E+00	8,61E-01	9,90E-02	6,90E-02	9,00E-03	5,10E-02	5,10E-02	5,10E-02
Right edge								
% error_edge (4 nodes)	8,32E+00	2,08E+00	2,80E-01	4,00E-02	0,00E+00	0,00E+00	0,00E+00	0,00E+00
% error_edge (8 nodes)	9,32E+00	2,80E-01	8,00E-02	0,00E+00	0,00E+00	0,00E+00	0,00E+00	0,00E+00

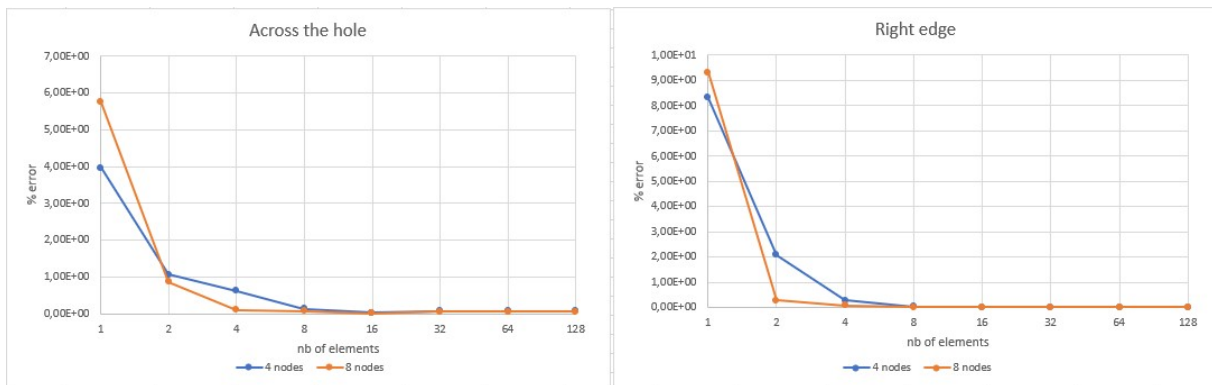


FIGURE 4: Graphs of the percentage error as a function of the number of elements per edge

For 8-node elements, the percentage of error decreases much faster as the number of elements increases than for 4-node elements. Moreover, the percentage of error is less than 1% as soon as the number of elements per edge is higher than 4 for all cases. Convergence in the mesh thus seems to be quite fast, and it is preferable to choose elements with 8 nodes rather than 4 nodes.

3.2 Stress concentration factor K

Now, let's introduce the stress concentration factor K for static load, defined as the relation of the actual maximum stress in the discontinuity and the average stress. It is given by the formula :

$$K = \frac{\text{Actual maximum stress}}{\sigma_{\text{calculated}}}$$

In order to choose the optimal number of elements for the simulations, let's calculate K as a function of the number of elements per edge with the software. As the maximum of stress is always close to the hole, it is possible to calculate K by dividing this maximum by $\sigma_{\text{across hole}}$. The results are displayed in the table and on the graph in Figure 5.

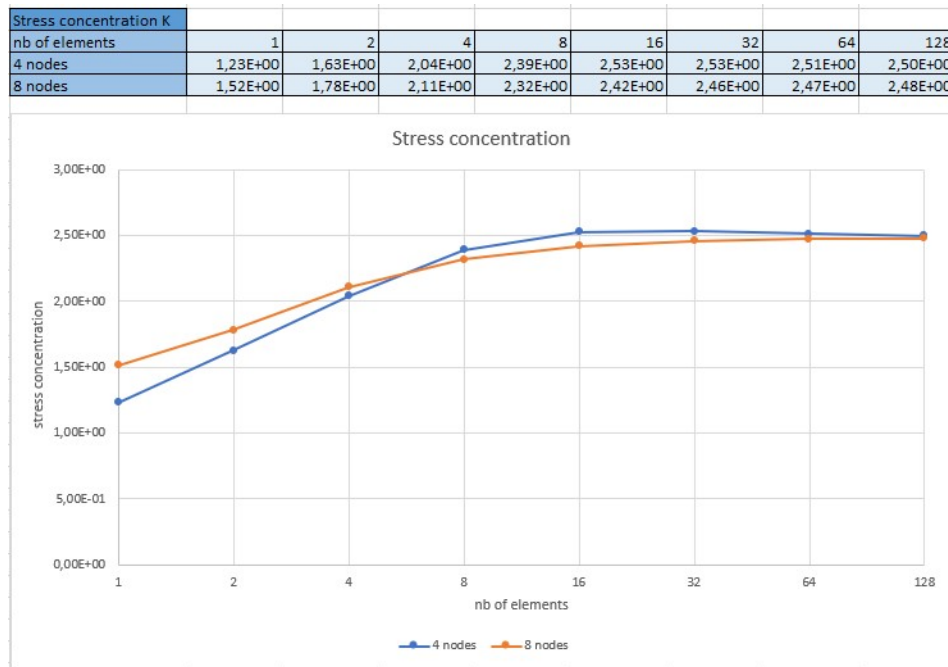


FIGURE 5: Stress concentration factor K as a function of the number of elements per edge

The K factor seems to converge towards the value 2.48, and more rapidly for 8-node elements than for 4-node elements. The simulation with 64 elements seems to give a satisfactory approximation of this result, as it seems that the asymptotic region of uniform convergence rate is reached from 64 elements. Thus, in the following, the simulations with ANSYS will be done with 64 8-node elements per edge.

According to the theory of stress concentration factors [1], for an infinitely large plate, the theoretical value of K should be 3. Now, still according to the theory, for a finite-width thin element with a circular hole, the K factor varies as a function of the d/H ratio (with d the diameter of the hole and H the width of the plate) according to the following equation :

$$K = 2 + 0.284 \left(1 - \frac{d}{H}\right) - 0.600 \left(1 - \frac{d}{H}\right)^2 + 1.32 \left(1 - \frac{d}{H}\right)^3$$

Let's try to reproduce this equation with the results obtained with ANSYS. For this, the simulations are run for a d/H ratio varying between 0.05 and 0.5. For simplicity, between each simulation, only the size of the hole is changed and the width of the plate is always equal to 0.04 m. The average stress is then equal to $\frac{\text{force}}{\text{cross section area}}$ where cross section area = area of the plate - area of the hole. The results are displayed in the table and on the graph in Figure 6.

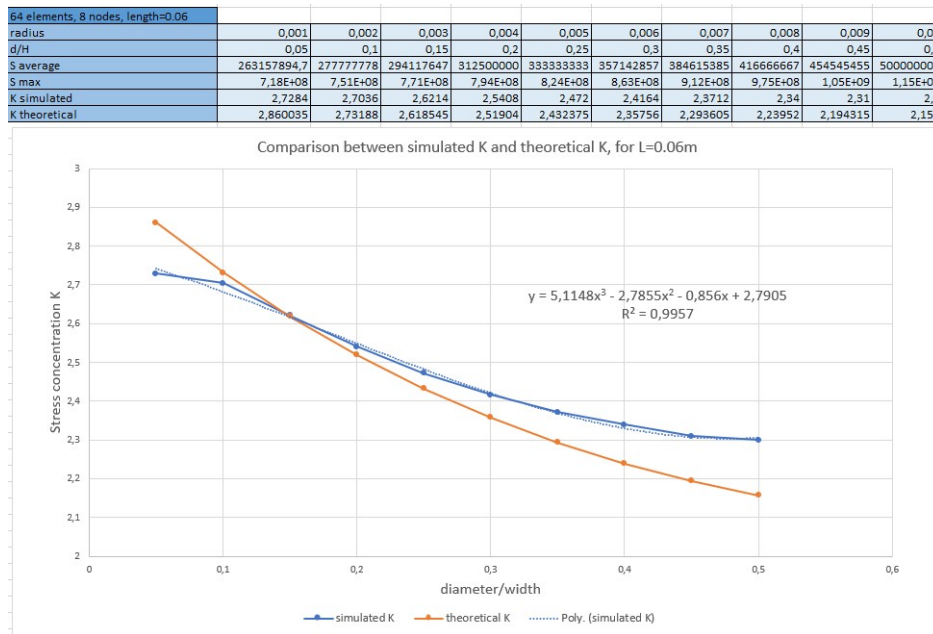


FIGURE 6: Graph comparing the simulated and theoretical K factors, as a function of the d/H ratio

According to the graph, the simulated K curve, whilst close to the theoretical curve, is quite different at the two ends. After some research, it seems that the problem comes from the fact

that in the theory the plate has an infinite length, which is not the case in this simulation. Let's do a sensitivity study with different length/width ratios in order to find the optimal length of the plate.

For simplicity, only the length is changed and not the width of the plate (always equal to 0.04m). The d/H ratio is left at 0.25, so the average stress will always be 333.33 MPa and the theoretical K is 2.432375. The percentage of error is calculated for each value of L/H with the formula $\%error = \frac{K_{simulated} - K_{theoretical}}{K_{theoretical}} \times 100$. The results are listed in Figure 7.

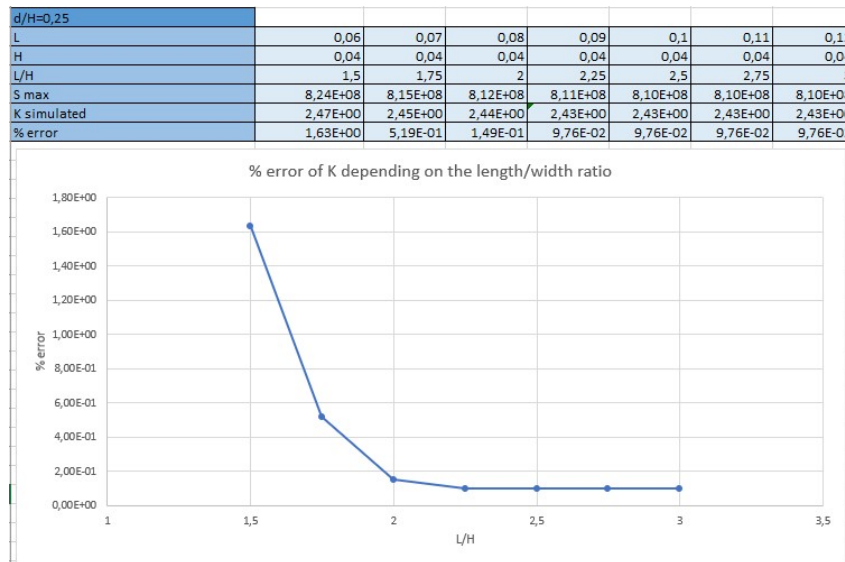


FIGURE 7: Percentage error of K depending on the length/width ratio

According to the graph, the % error is less than 0.2 for an L/H ratio greater than 2. In the following, let's see what the simulated K curve looks like for an L/H ratio of 2 and 2.5, which corresponds to a plate length of respectively 0.08m and 0.1m.

The same simulations as for Figure 6 are run, and the results are displayed in the table below and on the graph in Figure 8.

64 elements, 8 nodes										
radius	0,001	0,002	0,003	0,004	0,005	0,006	0,007	0,008	0,009	0,01
d/H	0,05	0,1	0,15	0,2	0,25	0,3	0,35	0,4	0,45	0,5
S average	263157894,7	277777778	294117647	312500000	333333333	357142857	384615385	416666667	454545455	500000000
K theoretical	2,860035	2,73188	2,618545	2,51904	2,432375	2,35756	2,293605	2,23952	2,194315	2,157
S max, length/width=1.5	7,18E+08	7,51E+08	7,71E+08	7,94E+08	8,24E+08	8,63E+08	9,12E+08	9,75E+08	1,05E+09	1,15E+09
K simulated, length/width=1.5	2,7284	2,7036	2,6214	2,5408	2,472	2,4164	2,3712	2,34	2,31	2,3
S max, length/width=2	7,15E+08	7,48E+08	7,66E+08	7,86E+08	8,12E+08	8,45E+08	8,86E+08	9,40E+08	1,01E+09	1,09E+09
K simulated, length/width=2	2,717	2,6928	2,6044	2,5152	2,436	2,366	2,3036	2,256	2,222	2,18
S max, length/width=2.5	7,13E+08	7,48E+08	7,66E+08	7,86E+08	8,10E+08	8,43E+08	8,84E+08	9,36E+08	1,00E+09	1,09E+09
K simulated, length/width=2.5	2,71E+00	2,69E+00	2,60E+00	2,52E+00	2,43E+00	2,36E+00	2,30E+00	2,25E+00	2,20E+00	2,18E+00

Comparison between simulated K and theoretical K for different length/width ratios

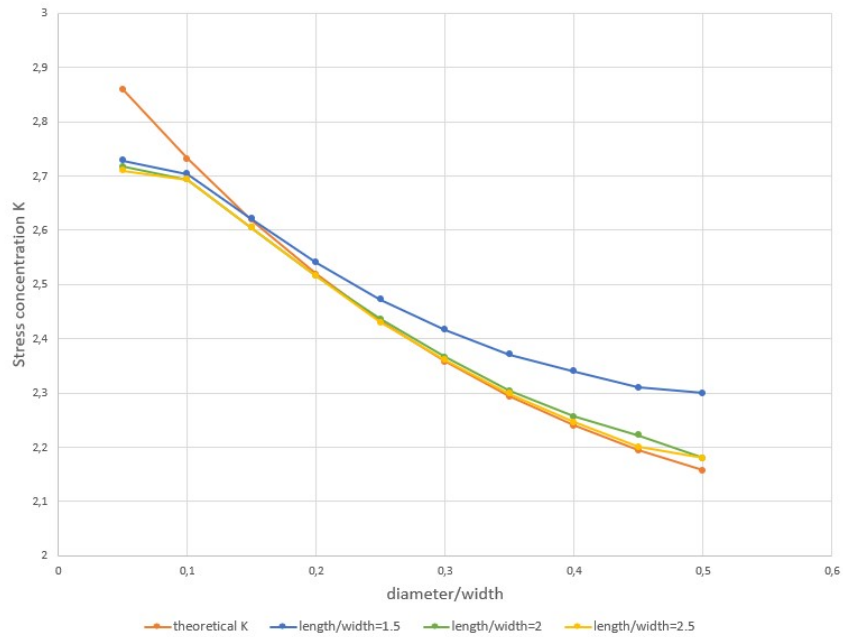


FIGURE 8: Graph comparing the simulated and theoretical K factors, for three different L/H ratios

The higher the L/H ratio, the closer the simulated K curve is to the theoretical K curve. Thus, with a length of 0.1m, the simulated K curve is much closer to the theoretical K curve than for a length of 0.06m. There are still some problems at the ends of the curves, as the simulated curves are no longer close to the theoretical curve. The problem will surely be solved if the plate has an infinite length, which is not possible with the software.

3.3 Improvement of the mesh

Several weeks after doing this study, and after gaining some experience with ANSYS, it seemed worthwhile to revisit the study to understand why the simulated values did not exactly match the theoretical values. This was facilitated by the use of the ANSYS APDL code.

After running the simulation for the same parameters as before to obtain the Figure 8, it appeared that there was an error message concerning the shape of the elements for certain values of the d/H ratio. Indeed, the mesh used was badly realized : for a too small radius of the hole (i.e. a small d/H ratio, which corresponds to the left-end side of the curves), the elements were deformed, they did not have a square shape anymore. Deformed elements can cause problems in the Jacobian matrix during calculations, which can lead to bad simulation results. To verify that the problem was indeed with the mesh, another improved mesh was made, as shown in Figure 9.

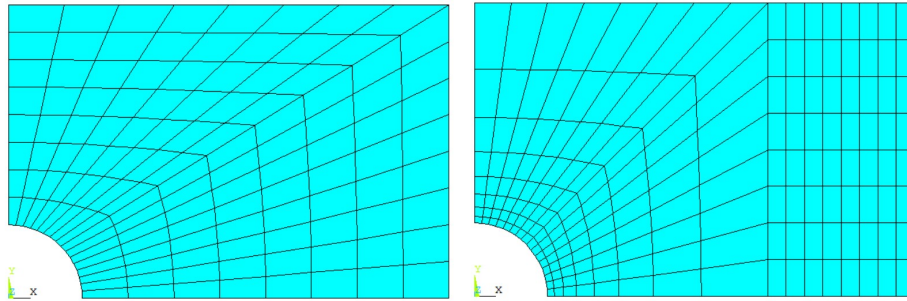


FIGURE 9: Comparison of two meshes : simple on the left and improved on the right

As seen in the figure, this new mesh is better than the previous one because the elements near the hole keep their square shape. Furthermore, the diagonal of the mesh no longer runs through the whole plate but only through a square whose dimensions remain the same in all simulations. Thus, even when the length of the plate changes, the elements will not be deformed. This mesh has been made with a spacing ratio of 0.1 for the two lines next to the hole and for the diagonal, so that the length of the elements is smaller near the hole, which will give a better result.

With 64 elements per line with the new mesh, the simulations give the result shown in Figure 10.

This time, the simulated results are much more satisfactory : there are no more problems at the ends of the curves and for a sufficiently large L/H ratio (i.e. a very long plate) the simulated curve lies perfectly on the theoretical curve. This study highlights the importance of meshing, a step that should not be neglected to obtain good simulated results.

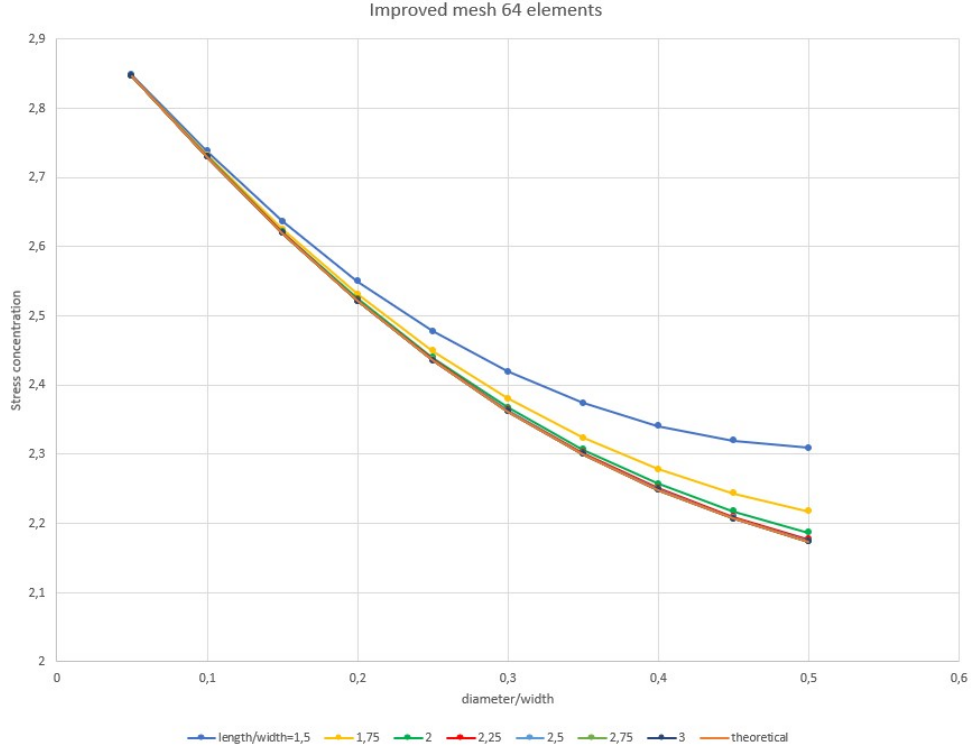


FIGURE 10: Graph comparing the simulated and theoretical K factors, with an improved mesh

To draw an interesting result from this study that could benefit practising engineers, let's plot a graph showing the error made in calculating the stress concentration factor K of a plate with a hole using the theoretical curve, as a function of different L/H and d/H ratios. This is shown in Figure 11.

This graph represents the percentage error between the simulated and theoretical K values, calculated according to the following formula : $\%error = \frac{K_{theoretical} - K_{simulated}}{K_{theoretical}}$. For a length/width ratio greater than 2, the error is less than 1% for any diameter/width ratio, so it is safe to use the theoretical K in these cases. However, for a L/H ratio of less than 2, the error can range from 2% to 7%. As the simulated K values are higher than the theoretical ones when the error is large (see Figure 10), it can be dangerous to use the theoretical solution as it will lead to an underestimation of the true value of the stress concentration in the plate. Thus, it is not advisable to use the theoretical formula when the error is too large, or else keep in mind that the stress concentration is underestimated.

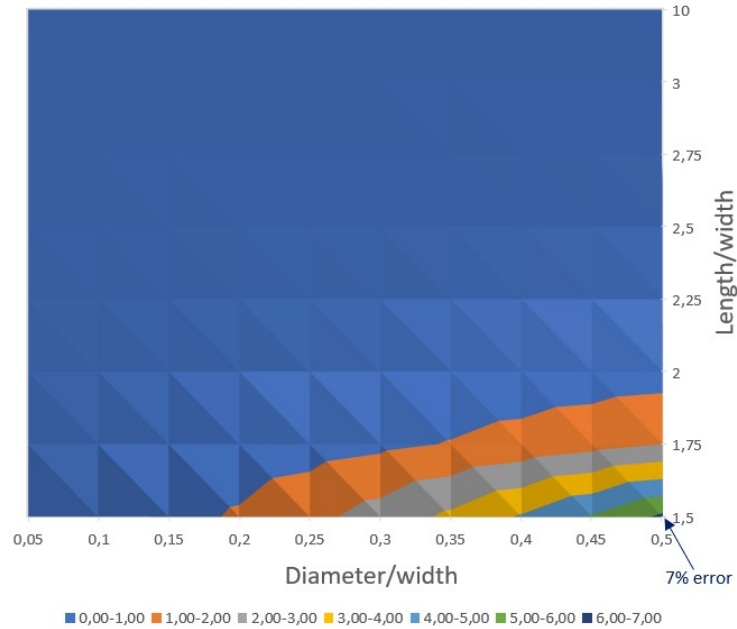


FIGURE 11: Percentage error made in calculating the K factor with the theoretical solution, for a plate with a hole

In this problem, a mesh convergence study was undertaken and this showed why it is important in order to have valuable results. The average stress and the stress concentration factor K were defined, and it was possible to compare the simulated K and the theoretical K . After seeing that the result depended on the length of the plate, it was made clear that the simulated values of K were closer to the theoretical ones when the L/H ratio was higher. This study showed how important it is to verify a result by the theory, and how to find a solution when the results do not match.

4 Introduction to the Lamé equations on a cylinder

The following study was conducted to compare two elements : the conforming finite element (CFE) which is used by the vast majority of commercial FE software nowadays, and the Lamé finite element (LFE) which was developed by Angus Ramsay [2]. The study of examples, notably of pressurised thick cylinders, will show why the LFE is interesting to use and sometimes even preferable to the CFE.

The Lamé finite element, as its name suggests, is based on the Lamé equations. Let's consider a uniform thickness axisymmetric body with a constant angular velocity ω , in a cylindrical coordinate system r, θ . The material considered has a Young's modulus E , a Poisson's ratio ν and a mass density ρ . The Lamé equations are then written :

$$\sigma_r = a - \frac{b}{r^2} - (3 + \nu) \frac{\rho \omega^2 r^2}{8}$$

$$\sigma_h = a + \frac{b}{r^2} - (1 + 3\nu) \frac{\rho \omega^2 r^2}{8}$$

with σ_r the radial stress, σ_h the hoop stress, and a and b the two Lamé coefficients determined from the boundary conditions.

4.1 First use of the LFE software

Now let's use the LFE software, developed by Angus Ramsay, on a specific problem : the pressurised thick cylinder. The cylinder considered has an inner radius $r_i = 0.1m$, an outer radius $r_o = 1m$ and an axial thickness $t = 0.01m$. The material considered has a Young's modulus $E=200GPa$ and a Poisson's ratio $\nu = 0.3$. There are an internal pressure p_i and an external pressure p_o applied on the cylinder.

Let's consider two load cases (LC1 and LC2) as defined in the tables below :

LC1	a (kPa)	b (kN)	f_i (kN)	f_o (kN)	p_i (kPa)	p_o (kPa)
	100	0	-2π	$+20\pi$	-100	100
LC2	a (kPa)	b (kN)	f_i (kN)	f_o (kN)	p_i (kPa)	p_o (kPa)
	0	100	$+20\pi$	-2π	10000	-100

The simulation is done with ANSYS and the LFE software for 8 nodes. For ANSYS, an axisymmetric shell is used and the bending part of the element is switched off. The results for each case are displayed in Figure 12 and 13.

The elastic solution given by the LFE software is the exact solution, no matter how many nodes are used. On the LC1 graph, it can be seen that the solution given by ANSYS for the radial stress and the hoop stress is exactly equal to the LFE solution.

Then, on the LC2 graph, it can be seen that the solution given by ANSYS is far from the exact

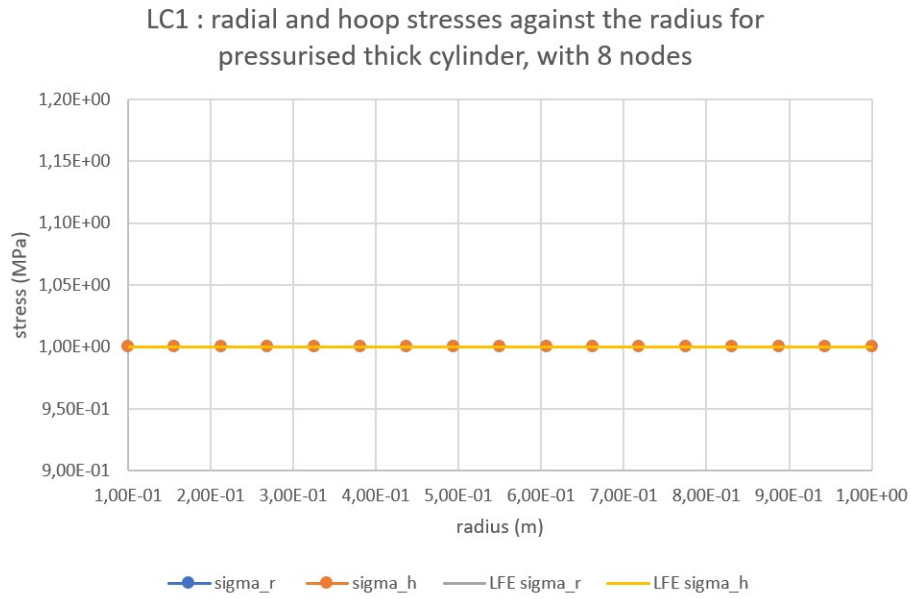


FIGURE 12: Radial and hoop stresses against the radius for pressurised thick cylinder, LC1

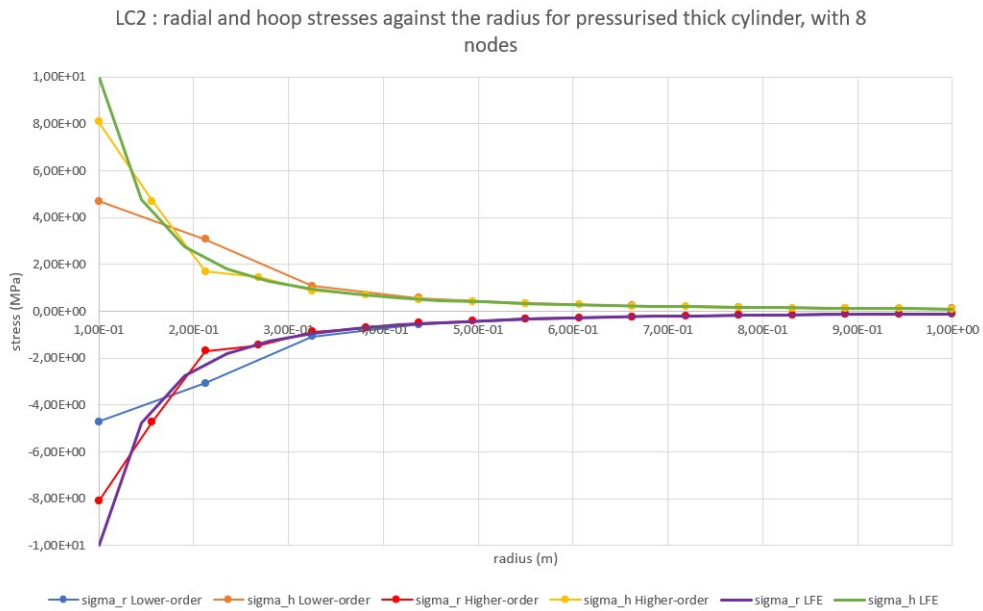


FIGURE 13: Radial and hoop stresses against the radius for pressurised thick cylinder, LC2

solution for a small radius. However, it is important to note that the higher-order solution is closer to the LFE solution than the lower-order solution, and if the number of nodes is increased then the solutions given by ANSYS will be much closer to the exact solution than with only eight nodes. An interesting property of the Lamé equations is that in the absence of body and thermal loading, it can be verified that at any points $\sigma_r + \sigma_h = 2a$. That is particularly visible on the LC2 graph, where $a=0$.

4.2 Mesh convergence study

Now, let's verify the convergence of elastic stress and plastic load factor for LC2.

First, a mesh convergence study was conducted with ANSYS, using lower-order and higher-order CFE, to check the convergence of elastic stress. The percentage error in stress has been calculated at the inner radius, as this is where the stress is maximal. The results of that study are shown in Figure 14.

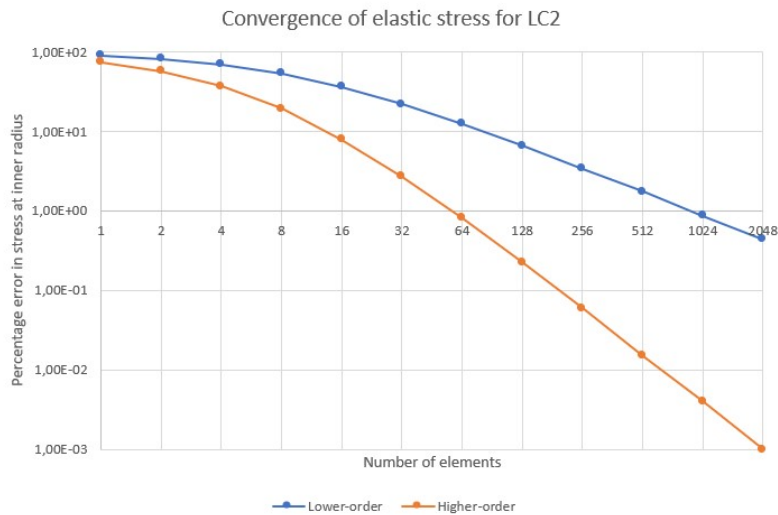


FIGURE 14: Convergence of elastic stress for LC2

The study was not done using LFE, as the elastic solution given by the LFE software is exact and does not depend on the number of elements (the percentage error is always equal to zero). Furthermore, the percentage error for the higher-order elements decreases faster than for the lower-order elements, and the error is less than 1% beyond 64 elements for the higher-order : a significant

number of elements are required before having a satisfactory error percentage. In this example, it is clear that LFE is preferable to CFE.

Then, a mesh convergence study was conducted to check the convergence of plastic load factor for LC2. For this study, the ANSYS software and the LFE software were used, as the plastic solution given by LFE is not exact. The results of that study are shown in Figure 15.

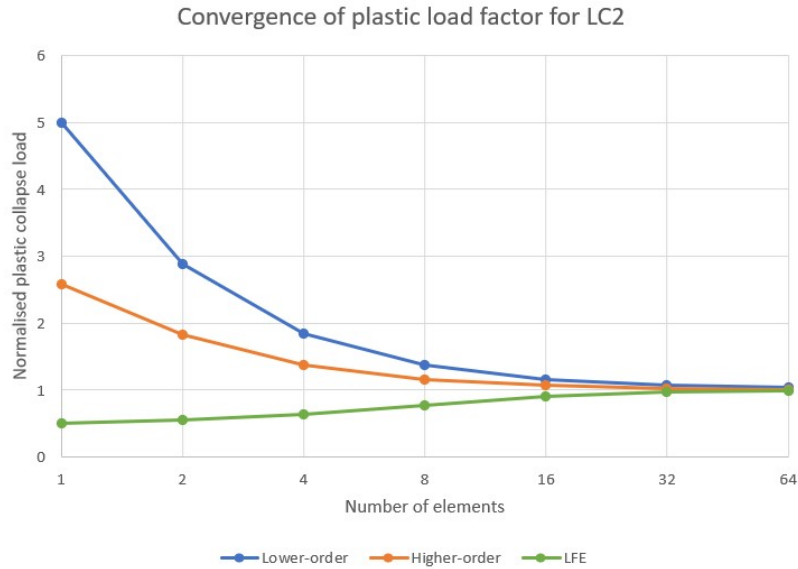


FIGURE 15: Convergence of plastic load factor for LC2 (von Mises criterion)

The exact value for the plastic collapse load is taken equal to 0.11601, it is the value obtained for 2048 elements. The normalised plastic collapse load is then equal to the load factor for a given number of elements, divided by 0.11601.

As seen on the graph, both the lower-order and the higher-order elements converge from below the true values. It means that the CFE under predict the exact stress, which can be dangerous if an engineer uses a coarse mesh and does not realise his mistake. However, the LFE converges from above the true values, which means that it will over predict the exact stress. So, even with a coarse mesh, the results will lead to a safe design. In this example, the LFE is also preferable to CFE.

4.3 Thick-walled internally pressurised cylinder

In the rest of this study, a problem of dimensioning a thick-walled pressurised cylinder of inner radius r_i and outer radius r_o is presented. The LFE software will be used in particular, but a comparison of this software with ANSYS will also be presented later. A limit to the Lamé equations will be highlighted by this study, among other findings.

In structural engineering, there are different methods of dimensioning a part or an element of a structure. One of them is the limit state design (LSD). In this method, the structure must satisfy two criteria : the serviceability limit state (SLS) and the ultimate limit state (ULS). These two criteria will be used in the following for our cylinder sizing study.

4.3.1 Design chart

In a thin-walled internally pressurised cylinder, it is assumed that the hoop stress is constant across the thickness of the cylinder wall and that there are no radial stress. However, in a thick-walled internally pressurised cylinder, the radial stress σ_r and the hoop stress σ_h vary through the wall thickness and they are principal stresses as there are no shear stresses [3]. Those two stresses are given by the Lamé equations as seen above. The difference between thick-walled and thin-walled cylinders is shown in Figure 16.

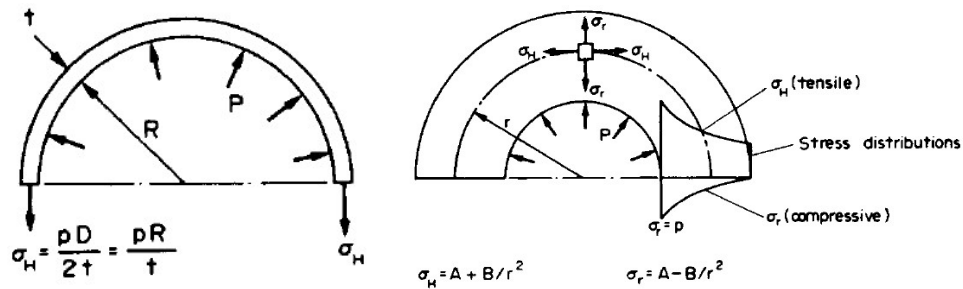


FIGURE 16: Comparison of stresses in thin-walled and thick-walled cylinders, [3]

In order to know which theory to use between the thin-walled and the thick-walled theory, let's introduce the K factor which is equal to D/t , where D is the inside diameter and t is the thickness of the cylinder. Since the maximum hoop stress is normally the limiting factor, it is this stress

which will be considered [3]. The hoop stress from the two theories is plotted for various D/t ratio, as well as the percentage error involved in using the thin cylinder theory, which is shown in Figure 17.

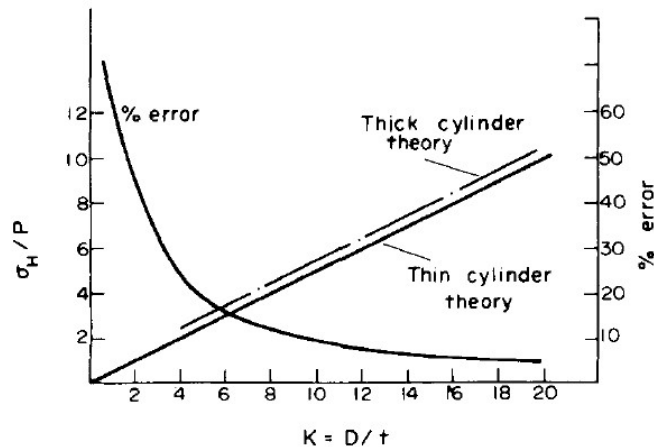


FIGURE 17: Comparison between thick-walled and thin-walled cylinder theory, [3]

As expected, the percentage error is maximal for a minimal factor K, since the smaller K is, the greater is the thickness t of the cylinder. In the following, only thick-walled cylinders will be used.

Now, let's introduce some quantities [4] :

- S_y is the uniaxial yield stress for the pipe material
- p is the pressure that causes yield up to some radius r_p , $r_i \leq r_p \leq r_o$, when using the Tresca criterion : $p = S_y \times \left(\frac{1}{2r_o^2} (r_o^2 - r_p^2) - \ln\left(\frac{r_i}{r_p}\right) \right)$
- p_e is the Elastic Limit Pressure, given by the p equation where $r_p = r_i$: $p_e = S_y \times \left(\frac{1}{2r_o^2} (r_o^2 - r_i^2) \right)$
- p_p is the Plastic Limit Pressure, given by the p equation where $r_p = r_o$: $p_p = S_y \times \left(-\ln\left(\frac{r_i}{r_o}\right) \right)$

To be able to work with a wide variety of cylinders, it can be interesting to introduce non-dimensional quantities, so the equations and results found will be applicable to different geometries.

To that extent, let's introduce the quantities as follow :

- the pressure load factor $P = \frac{p_p}{p_e}$, where $P \geq 1$
- the radius ratio $R = \frac{r_i}{r_o}$, where $0 < R < 1$
- the material yield stress $L = \frac{p_e}{S_y}$

$$- K = \frac{p_p}{S_y}$$

By introducing these quantities into the equations of p_e and p_p , R and P can be determined respectively from the SLS condition and the ULS condition : $R = \sqrt{1 - 2L}$ and $P = \frac{2\ln(R)}{(R^2 - 1)}$. Now, let's introduce the expression of R in the equation of P to have R and P as a function of L : $P = \frac{-\ln(1-2L)}{2L}$. Those equations for R and P are design equations. They were used, as well as the LFE software, to plot the graph in Figure 18.

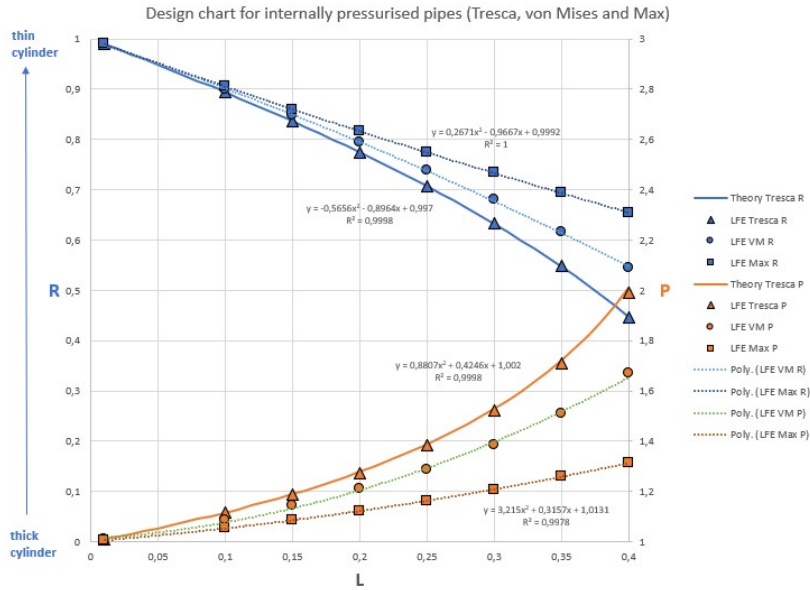


FIGURE 18: Design chart for internally pressurised pipes

The solid curves represent the theoretical values of R and P obtained with the Tresca criterion, they were obtained from the design equations for L ranging from 0.01 to 0.4. For the other curves, here is how they were obtained :

With a given S_y and a given L ranging from 0.01 to 0.4 p_e can be deduced, which is equal to $L \times S_y$. Knowing the cross-section area A of the cylinder ($A = 2\pi r_i t$), the force F to be applied inside the cylinder for each L can be deduced, since $F = A \times p_e$.

Now, using the LFE software, the force calculated as above is entered, r_i is set to 0.1m and r_o is varied so as to have an elastic load factor equal to 1 to at least 5 decimal places. For this step, it is possible to look for the outer radius by hand by section method, but the LFE software can also do it and more quickly. After finding r_o , R can be obtained, which is equal to r_i/r_o .

Then, to find P, it can be stated that $P = \lambda_p / \lambda_e$ where λ_p is the plastic load factor and λ_e is the elastic load factor. Since $\lambda_e = 1$, then P is simply equal to λ_p , which is given by the LFE software. These steps must then be repeated for each L and for the three different criteria, Tresca, von Mises and Maximum Principal Stress, which can be easily changed with the software.

Note : The R values are obtained from an elastic LFE analysis (because the elastic load factor was used). As the elastic result is exact regardless of the number of elements, a single element mesh could have been used to obtain these results. However, the P values are obtained from a plastic LFE analysis (because the plastic load factor was used). As the plastic solution is not exact, a refined LFE mesh was required to obtain accurate values. Meshes with 128 uniform length elements have been used here.

The values marked by triangles, circles and squares are the values of R and P obtained with the LFE software with respectively the Tresca criterion, the von Mises criterion and the Maximum Principal Stress criterion. As seen on the graph, the LFE Tresca values for R and P correspond perfectly to the Tresca theoretical curves, which verifies the values given by the software.

For the von Mises criterion and the Maximum Principal Stress criterion, it was not easy to find a theoretical solution : that is why the theoretical curves are not presented in this paper. However, a trend curve was made with Excel for these two criteria, whose equations are displayed on the graph along with the correlation coefficient.

According to the graph, it can be stated that for a given L, the Maximum Principal Stress criterion will lead to a greater R value (i.e. a smaller wall thickness of pipe) than for the von Mises criterion, which will lead to a greater R value than for the Tresca criterion. Likewise, for a given L, the Maximum Principal Stress criterion will lead to a lower P value than for the von Mises criterion, which will lead to a smaller P value than for the Tresca criterion.

It should also be noted that the graph stops at $L=0.4$. Indeed, the theoretical value of R and P with the Tresca criterion does not allow to go beyond $L=0.49$ because of the properties of the square root and the logarithm. Similarly, if the analysis with the LFE software is run for an L greater than 0.4, the graph in Figure 19 is obtained.

When L is equal to 0.45, it can be seen that the LFE value of P starts to diverge from the theoretical curve. The closer L gets to 0.5, the greater the gap between the theoretical and simulated values. For R, however, the simulated values seem to follow the theoretical curve (the last R point

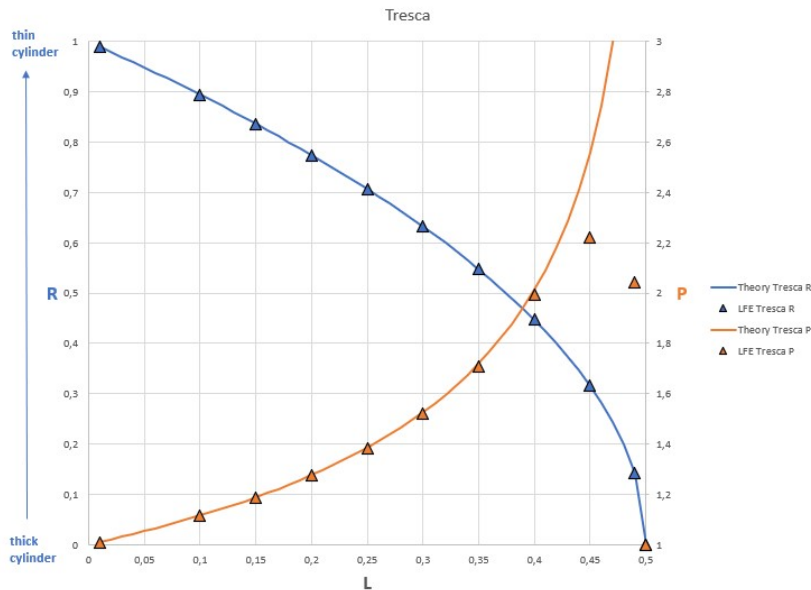


FIGURE 19: Tresca curves for L greater than 0.4

at $L=0.5$ can't be seen on the graph as it is hidden by the P point, but it has a value of 10^{-6}). This is due to the fact that P has been calculated with a plastic analysis, whereas R has been calculated with an elastic analysis.

4.3.2 Comparison of three yield criteria

Now, let's make a comparison of the three yield criteria. To do that, it is possible to plot each yield criterion on a single graph, with the normalised radial stress as the abscissa and the normalised hoop stress as the ordinate. This is shown in Figure 20.

The von Mises yield criterion is represented as an ellipse, the Tresca yield criterion is represented as a polygon and the Maximum Principal Stress criterion is represented as a square. This graph is particularly useful for determining whether a part is plastically deformed or remains in the elastic range under a given load. This is done by displaying the normalized radial and hoop stresses (which are the radial and hoop stresses divided by the yield stress) of the part on the graph. If the curve representing the stresses remains within the geometric shape of a given criterion, then the part remains elastic. However, if the curve goes on the geometric shape (partially or completely), then the part becomes plastic (partially or completely).

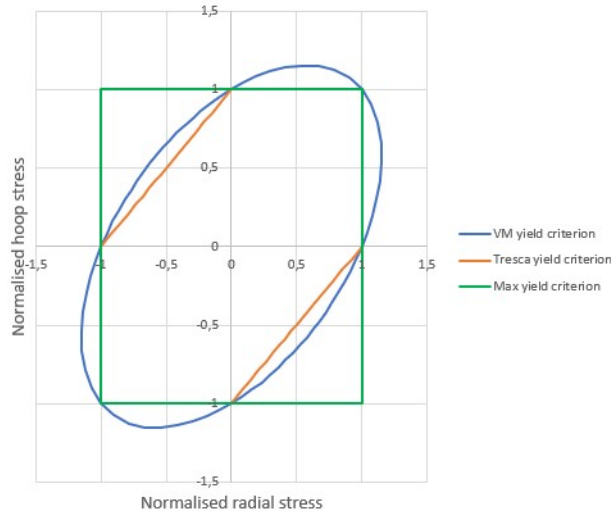


FIGURE 20: Three yield criteria on the same graph

The Tresca polygon being inscribed in the von Mises ellipse and in the Maximum Principal Stress square, it means that the limit pressures for the von Mises criterion and the Maximum Principal Stress criterion will be greater than or equal to those for Tresca.

Let's now apply this to the thick-walled internally pressurised cylinder problem. The simulation was run with the LFE software with 128 mesh elements, with an applied force of 10^6N , for a constant inner radius of 0.1m and an outer radius varying from 0.100001m to 1m. This corresponds to a variation of the ratio R from 0.1 to 0.99999. For each R, the simulations were run for the three different criteria. Their elastic and plastic load factor has been recorded, resulting in the table below.

	VM		Tresca		Max	
R	lambda_e	lambda_p	lambda_e	lambda_p	lambda_e	lambda_p
0.1	9,88E-01	1,99E+00	8,55E-01	1,73E+00	1,69E+00	1,73E+00
0.3	9,07E-01	1,98E+00	7,86E-01	1,73E+00	1,44E+00	1,73E+00
0.35	8,73E-01	1,92E+00	7,58E-01	1,73E+00	1,35E+00	1,73E+00
0.4	8,34E-01	1,73E+00	7,26E-01	1,56E+00	1,25E+00	1,73E+00
0.5	7,41E-01	1,32E+00	6,48E-01	1,19E+00	1,04E+00	1,71E+00
0.75	4,15E-01	5,27E-01	3,78E-01	4,96E-01	4,84E-01	5,75E-01
0.9	1,72E-01	1,87E-01	1,64E-01	1,82E-01	1,81E-01	1,92E-01
0.99999	1,55E-05	1,51E-05	1,55E-05	1,46E-05	1,55E-05	1,46E-05

The elastic and plastic limit pressures are obtained by multiplying the applied pressure by the elastic or plastic load factor. As the same pressure was applied for all these cases, then it is enough

to compare the λ_e and the λ_p to compare the limit pressures between each criterion. As expected, the limit pressures for the von Mises criterion and the Maximum Principal Stress criterion are greater than or equal to those for Tresca, as the λ_e and λ_p are greater for those two criteria than for Tresca. The prediction of the collapse load will then be different depending on the criterion chosen, so use of an inappropriate yield criterion can, in general, lead to lack of economy or lack of structural safety. The criterion to be used must then be chosen with care.

The graphical representation of these simulations is shown in Figure 21 for the Tresca criterion. Similar results were obtained for the other two criteria.

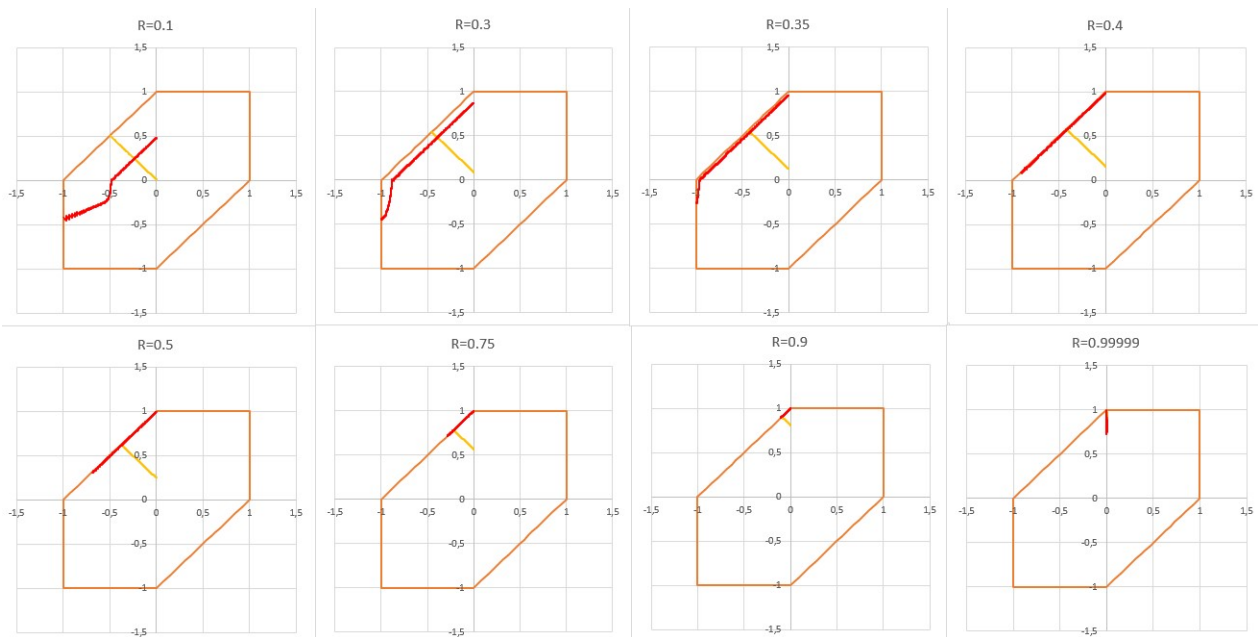


FIGURE 21: Evolution of the normalised stresses as a function of the R ratio for the Tresca criterion

The yellow curves represent the elastic solutions whereas the red curves are for the plastic solutions. The outer radius of the pipe is easily recognised as it lies on the line of zero radial stress and first plasticity develops at the inner radius of the pipe.

As seen on the figure, the plastic solution is superimposed on the yield criterion from $R=0.4$: the cylinder becomes fully plastic for $R=0.4$ for the Tresca criterion. But for the von Mises criterion, it becomes fully plastic for $R=0.35$ and for the Maximum Principle Stress criterion it is for $R=0.5$. This shows that, as said before, care must be taken in choosing the criterion to be used because

depending on whether Tresca, von Mises or Maximum Principle Stress is chosen, the conclusions may be different for the same cylinder.

It may also be interesting to note that, for all three criteria, the curve of the elastic solution makes an angle of 45 degrees with the x-axis for $R=0.1$. The bigger the R ratio is, the closer the elastic and the plastic curves are to the point $(0,1)$: the radial stress tends to zero and the hoop stress tends to 1 when R tends to 1. Furthermore, for a small R ratio, the hoop stress of the plastic solution is negative near the inner radius.

Comparing the results obtained with ANSYS and the LFE software, they are identical for $R=0.5$ and $R=0.9$. However, for $R=0.1$, the results are quite different as seen in Figure 22 for the von Mises criterion.

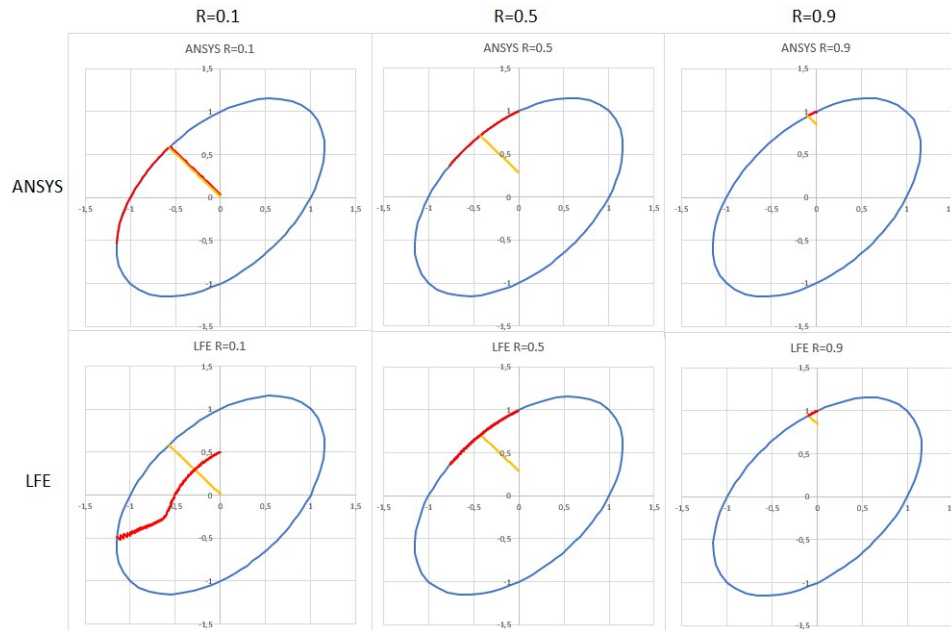


FIGURE 22: Comparison of the results obtained with ANSYS and the LFE software

For the plastic analysis with ANSYS, a force of 10^8 N was applied to the inner radius and a time step of 10000 was used. In addition, the mesh was made with 128 higher-order elements.

As the results for $R=0.5$ and 0.9 are the same, this gives us some confidence in the results obtained with the two software. However, for $R=0.1$, the difference in results could be explained by the fact

that the LFE software was incorrectly calibrated.

Note : An improvement would be to have a file allowing to give the elastic modulus, or to change the number of iterations of the LFE software which is for the moment maintained constant.

Another reason that could explain this difference between ANSYS and LFE is that in general it is assumed that the elasticity is linear. But when the strain exceeds 1%, one has to be careful because the elasticity can become non-linear. If the elasticity option is left on linear in ANSYS, this can lead to bad results : this may be the case for $R=0.1$ here. To verify that, let's focus on the maximum percentage strain in the cylinder at the elastic limit load, depending on the R ratio. After running the simulation on ANSYS with the same model as before and with 128 elements, the results are shown in Figure 23.

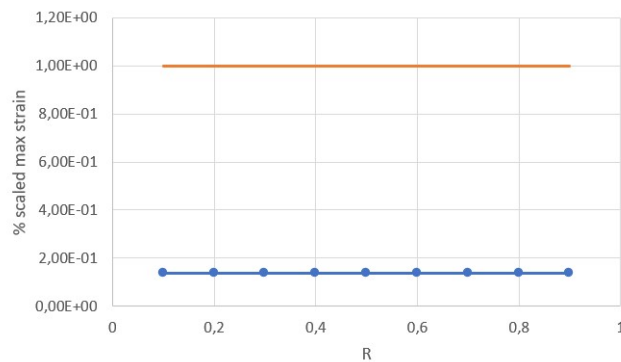


FIGURE 23: Maximum percentage strain in the cylinder

As seen on the graph, the percentage scaled maximum strain in the cylinder is always less than 1% regardless of R . This means that it is a false lead : the difference between ANSYS and LFE does not come from this issue.

In this study, the usefulness of the LFE software was shown in comparison to the ANSYS software, which uses the CFE. The thick-walled cylinder problem was also addressed, highlighting the use of the Lamé equations. By comparing three yield criteria for the same non-dimensional problem, it was shown that the choice of the yield criterion was very important. In particular, the Tresca criterion has a limit for calculating the parameter P when L is close to 0.5. Finally, when comparing the stresses obtained with ANSYS and the LFE software, the results are the same except for $R=0.1$, which seems to show a difference in behaviour between the two programs.

5 Rotors

The following study will focus on rotors and will use the Lamé equations introduced earlier. It is largely based on Vullo and Vivio's book [5] and reproduces many examples of it.

5.1 Rotating annular disk

First, let's focus on the hoop and radial stresses of a rotating disc of constant thickness, only subjected to centrifugal loading. The disc has the outer radius r_e and the inner radius r_i , it rotates at the angular velocity ω and it is made of a material of density γ , of Young's modulus E and of Poisson's ratio $\nu = 0.3$.

To have a more general model, let's introduce the dimensionless parameters :

$$- \beta = \frac{r_i}{r_e}$$

$$- \rho = \frac{r}{r_e}$$

as well as the variable $\sigma_0 = \gamma \omega^2 r_e^2$.

After calculations not detailed here, the general solutions below are obtained for the radial stress σ_r , the hoop stress σ_t and the displacement u :

$$\begin{cases} \sigma_r &= \frac{3+\nu}{8} \cdot \sigma_0 \cdot \left(1 + \beta^2 - \frac{\beta^2}{\rho^2} - \rho^2 \right) \\ \sigma_t &= \frac{3+\nu}{8} \cdot \sigma_0 \cdot \left(1 + \beta^2 + \frac{\beta^2}{\rho^2} - \frac{1+3\nu}{3+\nu} \cdot \rho^2 \right) \\ u &= \frac{r_e}{E} \cdot \rho \cdot \frac{3+\nu}{8} \cdot \sigma_0 \cdot \left[(1+\beta^2) \cdot (1-\nu) + (1+\nu) \cdot \frac{\beta^2}{\rho^2} - \rho^2 \cdot \left(\frac{1-\nu^2}{3+\nu} \right) \right] \end{cases}$$

The hoop stress decreases continuously from the inner radius to the outer radius, it is maximum at the inner radius and minimum at the outer radius. The minimum and maximum values of the hoop stress are given by the following formula :

$$\sigma_{t,\min,\max} = \left[\frac{1+\beta^2}{2} \mp \frac{1+\nu}{4} \cdot (1-\beta^2) \right] \cdot \sigma_0$$

where the plus sign applies for the inner radius and the minus sign for the outer radius.

To check that the same thing is obtained by simulation, the LFE software was used to draw the Figure 24.

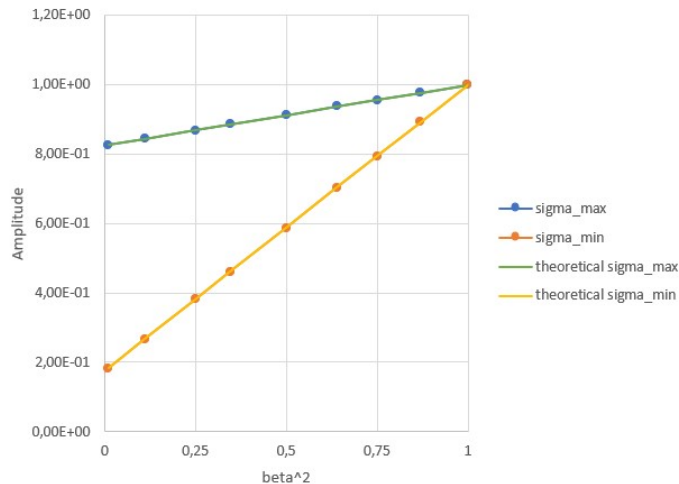


FIGURE 24: Distribution curves of dimensionless stresses $\sigma_{t,max}/\sigma_0$ and $\sigma_{t,min}/\sigma_0$ as a function of β^2 , for $\nu = 0.3$

The dimensionless stresses $\sigma_{t,max}/\sigma_0$ and $\sigma_{t,min}/\sigma_0$ were plotted on the graph as a function of the dimensionless parameter $\beta^2 = (r_i/r_e)^2$. The simulation was done for a density of 7500 kg/m^3 and an angular velocity of 6.28 s^{-1} . It can be seen that the simulated values are in perfect agreement with the theoretical values obtained from the previous formula, which makes it possible to verify the results obtained by the simulation.

After focusing only on the hoop stress, let's now focus on the hoop and the radial stress as a function of $\rho = r/r_e$. For that, let's use the theoretical solution for σ_r and σ_t as seen above. More precisely, let's use the expression in parentheses in those theoretical formula, by introducing the new variables $\tilde{\sigma}_r = \frac{8}{(3+\nu)} \frac{\sigma_r}{\sigma_0}$ and $\tilde{\sigma}_t = \frac{8}{(3+\nu)} \frac{\sigma_t}{\sigma_0}$. If the constant factor $\sigma_0(3+\nu)/8$ is not considered, these variables are therefore equivalent to σ_r and σ_t .

The simulation was done with the LFE software for different values of $\beta = r_i/r_e$ (0.25, 0.5 and 0.75), the results are shown in Figure 25.

The blue curves are the simulated results and the orange curves are the theoretical results. As seen on the graph, in this case the theoretical and simulated results also match perfectly which is reassuring.

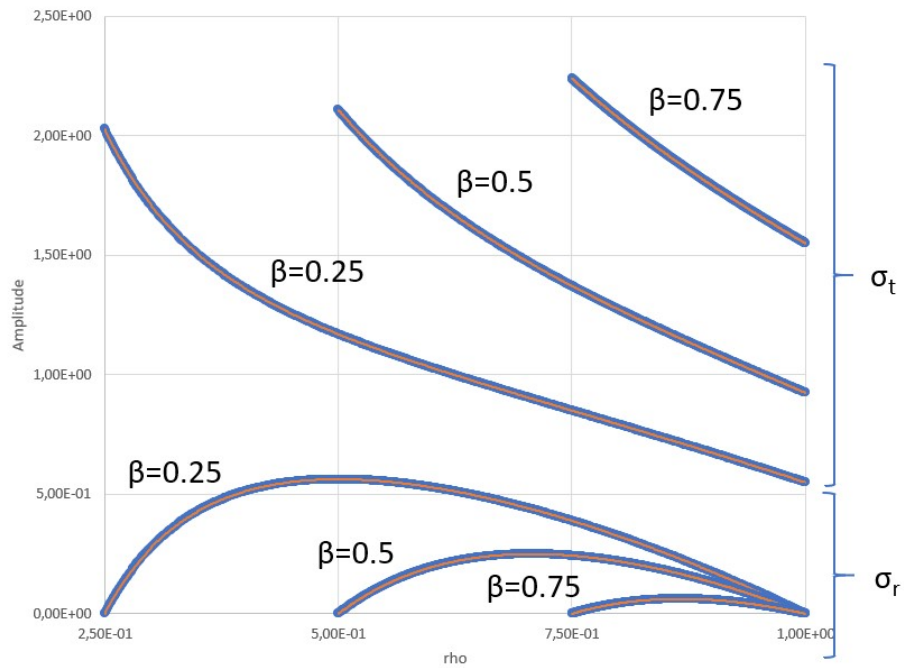
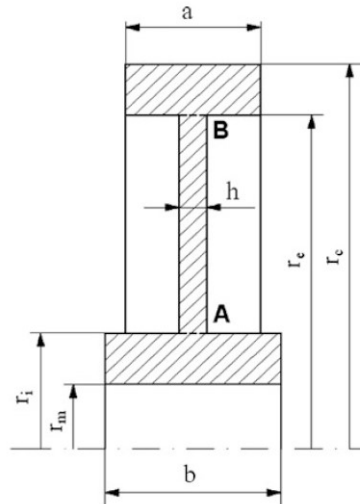


FIGURE 25: Distribution curves of dimensionless stresses $\tilde{\sigma}_r$ and $\tilde{\sigma}_t$ versus dimensionless radius, for different values of β

5.2 Three-part rotor only subjected to centrifugal loading

For this example, let's consider the following rotor :



It consists of three parts (a constant thickness disk, a hub and a crown ring) where the different radius are $r_m = 0.05$ m, $r_i = 0.09$ m, $r_e = 0.26$ m and $r_c = 0.3$ m and where the different thickness are $a = 0.1$ m, $h = 0.020$ m and $b = 0.13$ m. The rotor is made of a material of density $\gamma = 7800 \text{ kg/m}^3$, of Young's modulus $E=210$ GPa and of Poisson's ratio $\nu = 0.3$, and has an angular velocity of $\omega = 2\pi \times 6000/60 \approx 628 \text{ s}^{-1}$.

After calculations not detailed here, the hoop and radial stresses in the disk of thickness h are given by :

$$\begin{cases} \sigma_r = 190.92 + 5.88/\rho^2 - 85.87 \cdot \rho^2 \\ \sigma_t = 190.92 - 5.88/\rho^2 - 49.44 \cdot \rho^2 \end{cases}$$

Once again, let's compare these results to simulated ones using the LFE software. This is shown in Figure 26.

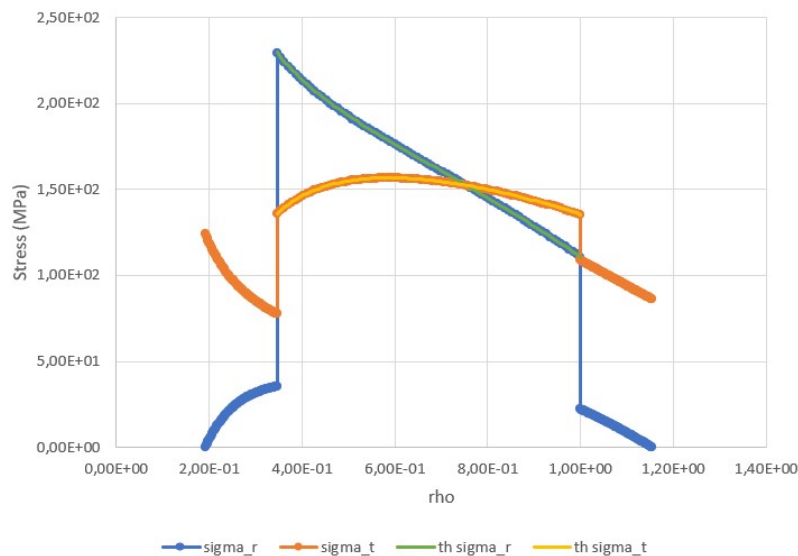


FIGURE 26: Distribution curves of stresses σ_r and σ_t versus dimensionless radius in the rotor

As seen on the graph, the stresses were plotted against the dimensionless radius $\rho = r/r_e$. For the disk of thickness h for which the theoretical solution is known, it can be seen that the theoretical curves (in green and yellow) and the simulated curves (in blue and orange) overlap perfectly for ρ between 0.35 and 1. Two steps can be seen in the stresses : this corresponds to the sudden change in thickness of the rotor.

A quick test to check that there are no errors in the simulation is to plot the radial force and the displacement along the radius, as seen in Figure 27.

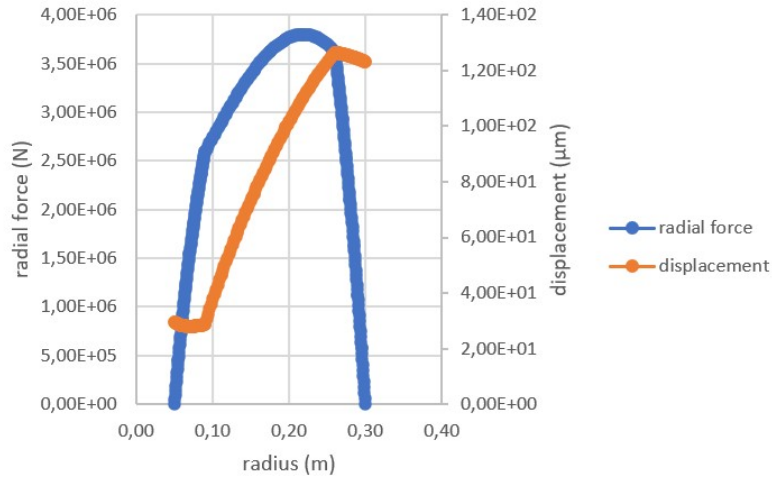


FIGURE 27: Radial force and displacement along the radius in the rotor

It can be seen that the radial force and the displacement are continuous along the radius of the rotor. This is a condition that must be met for the results to be valid, so there is no problem here.

5.3 Three-part rotor subjected to centrifugal loading and surface forces

Let's take the same rotor as before, but this time adding surface forces of -10 MPa and 40 MPa applied to hub radius r_m and crown ring radius r_c respectively. After calculations, the theoretical hoop and radial stresses in the disk of thickness h are given by :

$$\begin{cases} \sigma_r = 200.13 + 5.51/\rho^2 - 85.87 \cdot \rho^2 \\ \sigma_t = 200.13 - 5.51/\rho^2 - 49.44 \cdot \rho^2 \end{cases}$$

With the LFE software, a force F_1 was applied to the hub radius r_m where $F_1 = pressure \times area = 10 \times 10^6 \times 2\pi \times 0.05 \times 0.13 \approx 408 \text{ kN}$. A force F_2 was also applied to the crown ring radius r_c where $F_2 = 40 \times 10^6 \times 2\pi \times 0.3 \times 0.1 \approx 7.54 \text{ MN}$. All other parameters are taken as in the previous example. The results are shown in Figure 28.

As seen on the graph, the theoretical curves (green and yellow) and the simulated curves (blue and orange) are very different for ρ between 0.35 and 1. This can be for two different reasons : either the theoretical solution is wrong, or the simulated solution is wrong. Since the LFE software always gave the right result so far, it is not unlikely that an error occurred in the calculation of

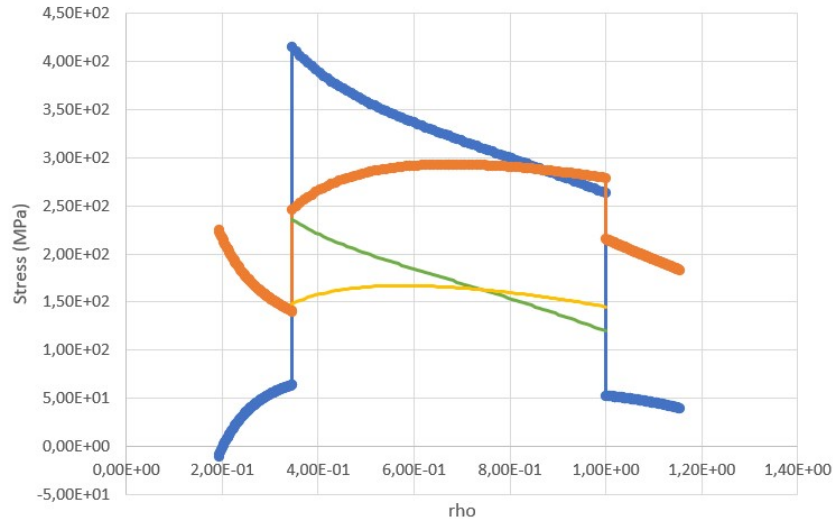


FIGURE 28: Distribution curves of stresses σ_r and σ_t versus dimensionless radius in the rotor

the theoretical formula for the hoop and the radial stresses. To check this, let's redo the simulation with another software to see what result is obtained.

For the new simulation, let's use ANSYS. Unlike the LFE software, the result given by ANSYS is not exact and there is therefore a need to conduct a mesh convergence study. To do this, let's redo the previous study of a three-part rotor only subjected to centrifugal loading for which the theoretical solution is known and agrees with the LFE simulation. This is shown in Figure 29.

The graph shows the percentage error between the simulated stress and the theoretical stress at the radius 0.09 versus the number of elements, where the percentage error is calculated according to the formula : $\%error = \frac{\sigma_{simulated} - \sigma_{theoretical}}{\sigma_{theoretical}} \times 100$.

The rate of convergence for the radial stress is also plotted on the figure. Let's call $\sigma_e|_m$ the percentage error calculated for the number of elements 2^m . The rate of convergence q is then given by the formula : $q = \frac{\log(\sigma_e|_{m+1}/\sigma_e|_m)}{\log(1/2)}$.

As seen on the graph, the error is less than 1% for both hoop stress and radial stress for a number of elements greater than 64. To do the next study with ANSYS, it will then be sufficient to use a mesh of 64 elements.

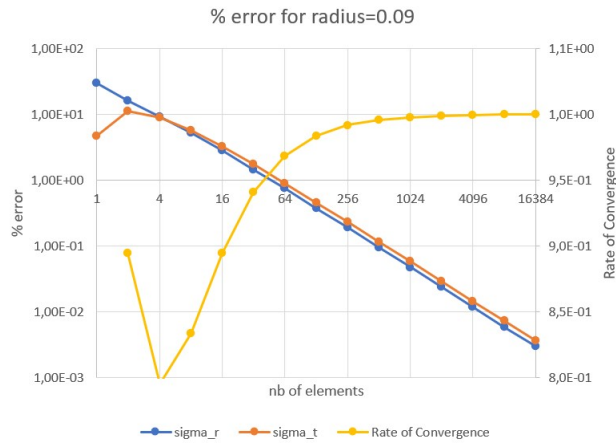


FIGURE 29: Mesh convergence study for the example of a rotor only subjected to centrifugal loading

The analysis with ANSYS was done with the same parameters as for the LFE analysis, and the results are shown in Figure 30.

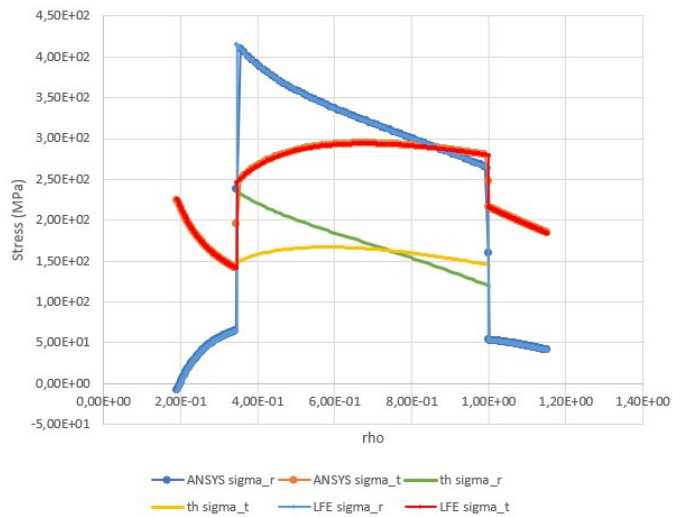


FIGURE 30: Distribution curves of stresses σ_r and σ_t simulated with ANSYS

The results obtained with ANSYS and LFE are exactly the same, but this is not very visible on the graph as the curves overlap perfectly. Thus, the simulation done with ANSYS validates the results obtained with the LFE software and it would seem that there is an error in the theoretical

formula for the hoop and radial stress in [5].

To evaluate the influence of the central disk's thickness h on its stress state, the book [5] offers a comparative study with three different values of h (0.020 m, 0.040 m and 0.080 m). As the theoretical formula is wrong for the stresses, the book's study is also wrong. That is why it has been redone with the LFE software, and the correct results are shown in Figure 31.

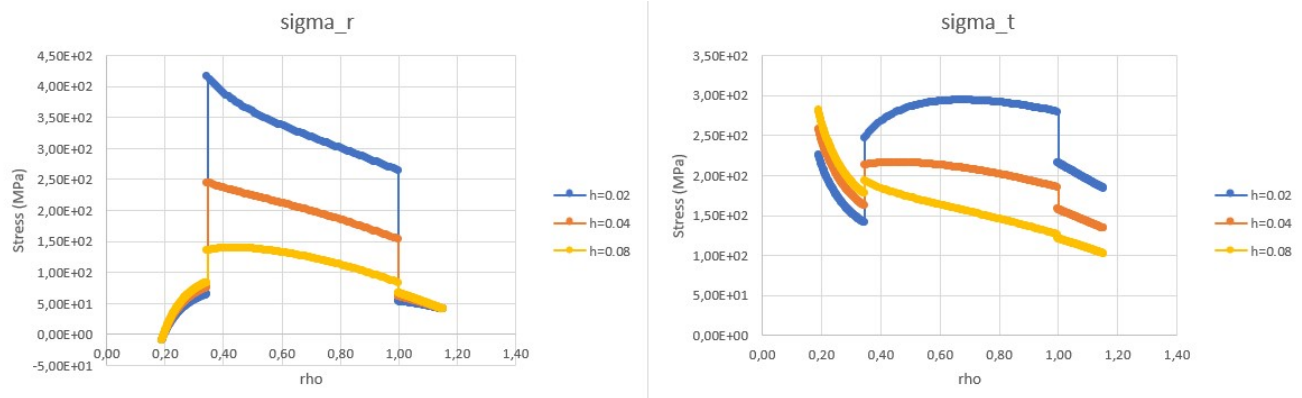
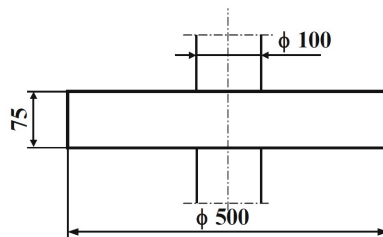


FIGURE 31: Distribution curves of stresses σ_r and σ_t versus dimensionless radius for different thicknesses h

As seen on the graph, h has a great impact on the stress state but also on the concavity of the curves. For the radial stress for ρ between 0.35 and 1, for example, the curve is convex for $h=0.08$ and concave for $h=0.02$, the opposite is true for hoop stress. For $h=0.08$, the hoop stress is always higher than the radial stress whereas for $h=0.02$ this is not always the case.

5.4 Annular disk assembled on a solid shaft with a shrink-fit

Let's consider an annular steel disk which is assembled on a solid shaft with a shrink-fit, as seen below.



The annular disk and the shaft are made of steel ($\gamma = 7.8 \times 10^3 \text{ kg/m}^3$, $E=200 \text{ GPa}$ and $\nu = 0.3$). The disk is of constant thickness $h=75 \text{ mm}$, of inside diameter $2r_i = 0.1 \text{ m}$ and of outside diameter $2r_e = 0.5 \text{ m}$. The shrink-fit generates a contact pressure $p_c = 100 \text{ MPa}$ at the disk/shaft interface when there is no angular velocity and when the assembly temperature is equal to the ambient temperature.

According to the theory, a contact pressure p_c generates a radial displacement u_d of the interface at the radius r_i of the disk and a radial displacement u_a at the radius r_i of the shaft. This results in a radial interference $i = u_d - u_a = 52.1 \text{ }\mu\text{m}$.

The problem is then modelled with the LFE software. For now, the angular velocity is kept at zero. In order to have a contact pressure p_c at the interface, let's use the equation : $\Delta r = r \times \alpha \times \Delta T$, where Δr is the change in radius and is equal to i , r is the interface radius and is equal to r_i , α is the coefficient of expansion and is taken equal to 1 and ΔT is the change in temperature. So, to have a pressure p_c at the interface, and if the temperature of the disc is 0 , then a temperature of $\frac{\Delta r}{r \times \alpha} = \frac{i}{r_i} = \frac{52.1 \times 10^{-3}}{50} = 0.001042$ must be applied to the shaft.

Then, the speed of the rotor is varied from 0 to 716 rad/s , value for which the contact pressure is theoretically zero. Let's call $\sigma_{t,p}$ the maximum hoop stress due to contact pressure, $\sigma_{t,\omega}$ the maximum hoop stress due to rotation only and σ_t the maximum total hoop stress at the disk's inner radius. These three quantities are a function a ω^2 , they are represented in Figure 32.

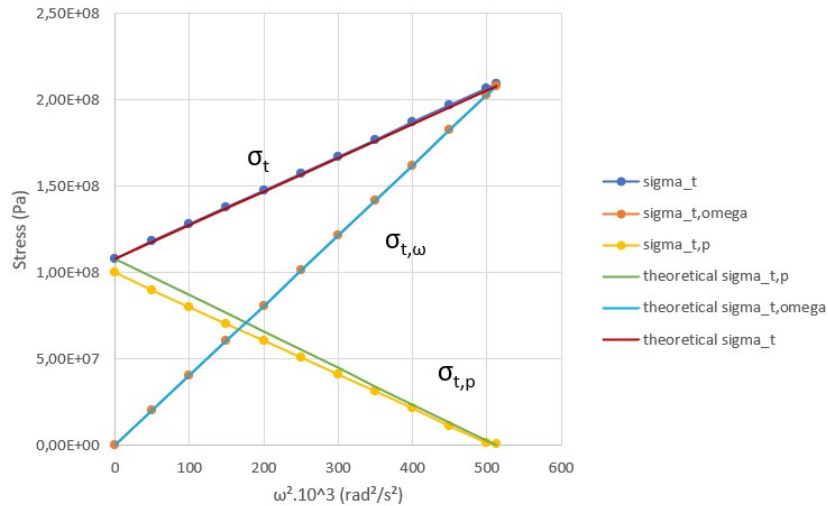
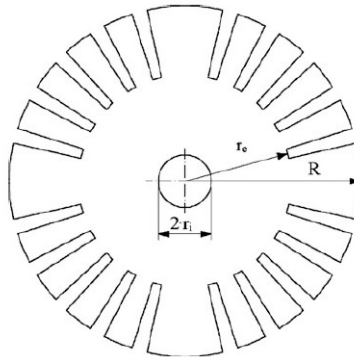


FIGURE 32: Different stresses (σ_t , $\sigma_{t,\omega}$ and $\sigma_{t,p}$) versus ω^2 in a shrink-fit shaft/disk assembly

As seen on the graph, the simulated curves are exactly the same as the theoretical ones except for $\sigma_{t,p}$ which is quite different on one end. The reason for this difference is not yet known.

5.5 Constant thickness disk with radial slots

This short study will mainly allow to better master ANSYS on a more complex model than all the previous ones. Let's consider a constant thickness disk with peripheral radial slots, whose geometry is shown below.



The radii of the disk as seen on the drawing are known : $r_i = 100 \text{ mm}$, $r_e = 400 \text{ mm}$ and $R = 660 \text{ mm}$. The rotor is made of a material of density $\rho = 7800 \text{ kg/m}^3$, of Young's modulus $E = 210 \text{ GPa}$ and of Poisson's ratio $\nu = 0.3$. It is only subjected to an angular velocity of 188.5 s^{-1} . The problem is circularly symmetrical, and for simplicity it will be assumed that all rotor sections are of the same size. With ANSYS, only one section will then be modelled, as seen on Figure 33.

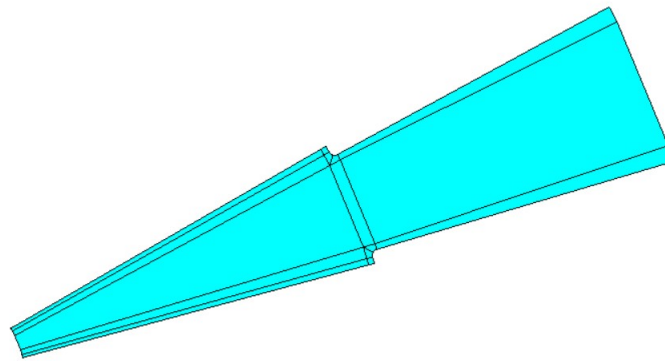


FIGURE 33: Modeling a disk with radial slots with ANSYS

The lines seen on the section separate different areas. It was necessary to create this area partition

so that each area is formed of exactly 4 lines : this will allow to have a good mesh with quadrilaterals rather than triangles, as they allow to have a more precise result. In particular, it is the geometry close to the 2 corners of the slot that determined the area partition. Indeed, this is where there will be a concentration of stress and it is therefore necessary to have a refined mesh so that the simulated result is close to the theory. One of the solutions is to create a square around each corner, so it will be possible to refine the mesh as desired. The optimised mesh is shown in Figure 34.

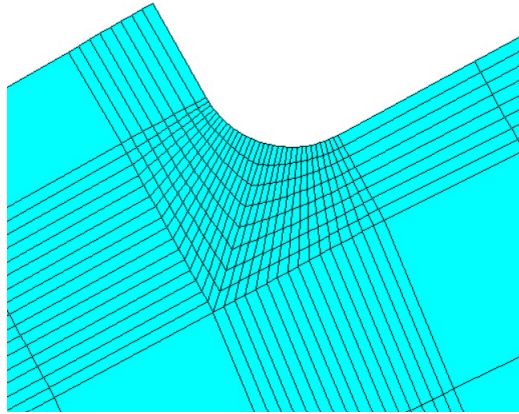


FIGURE 34: Optimised mesh of an angle of a slot

In addition, as can be seen in the figure, the angle is rounded : it was necessary to create a line fillet. Indeed, if we leave an angle of 90° , it will generate a singularity : the more the mesh is refined, the more the stress will increase to infinity. This is due to the fact that the theoretical solution can't take into account the stress at sharp angles. The difference in geometry between a 90° angle and a line fillet is shown in Figure 35.

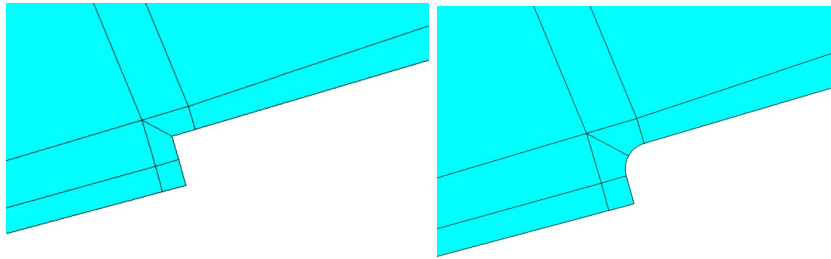


FIGURE 35: Comparison of two geometries of an angle of a slot

Then, a mesh convergence study was carried out on a model with line fillet and on a model with 90° angles to see the effect of a singularity. The maximum stress of the angle versus the number of elements per line is shown in Figure 36.

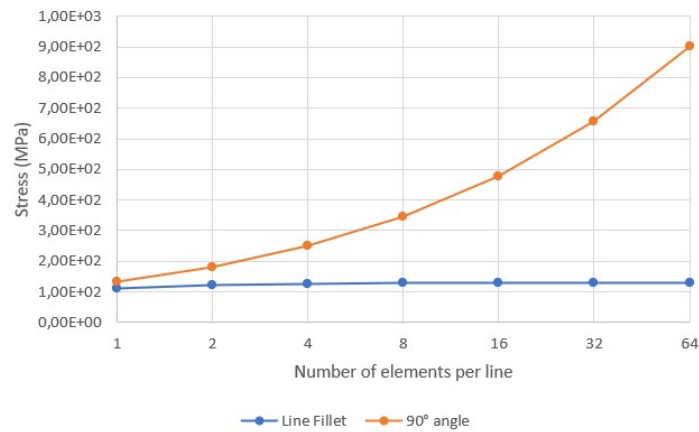


FIGURE 36: Mesh convergence study to show the effect of a singularity

As can be seen on the figure, as the number of elements increases, the stress increases a lot for the 90° angle model. For the line fillet model, on the other hand, the stress converges to a certain value as the number of elements increases. Here, it can be seen how important it is to make a line fillet to avoid singularities.

This study allowed to learn how to better use ANSYS on a complex case to model, unlike the other models where they are all very simple (just a plate or a beam). It also helped to learn how to make a nice mesh, that's usually the most time consuming. Also, it was seen the problem of singularities,

which occurs when there are right angles in the model. This can lead to misinterpretation if the stress increases despite a refined mesh. A good solution to this is to use a line fillet.

6 Commercial project

For the last project of the internship, I was able to work on a commercial project to verify that a balustrade complies with certain European standards. To do this, I first carried out a study on a simple model of the balustrade, in order to choose which ANSYS element to use next. The balustrade is thus modelled by a simply supported rectangular plate under UDL.

6.1 Simply Supported Rectangular Plate under UDL

In this technical note, a code verification study will be conducted on three different shell elements of the ANSYS software. The model used for this study will be a simply supported rectangular plate under uniformly distributed load, as the theoretical solution for this example is known.

6.1.1 Theoretical solution

The theoretical Navier plate solution will be used here. This solution is an infinite series that converges as the number of terms in the series is increased. A number of terms equal to 250 can be considered sufficient for the solution to be close to the exact solution. This number was chosen after a study on the convergence of the Navier plate solution [6].

To do the code verification, two quantities obtained with ANSYS will be compared to the theoretical solution : the principal moments M_1 and M_2 . The theoretical values for these quantities are given by the formula below [7] :

$$M_1 = \frac{M_x + M_y}{2} + \sqrt{\left(\frac{M_x - M_y}{2}\right)^2 + M_{xy}^2}$$
$$M_2 = \frac{M_x + M_y}{2} - \sqrt{\left(\frac{M_x - M_y}{2}\right)^2 + M_{xy}^2}$$

where

$$M_x = -D \times \sum_{m=1}^{250} \sum_{n=1}^{250} \left(\frac{\sin\left(\frac{n\pi y}{B}\right) \times (-16)q \sin\left(\frac{m\pi x}{A}\right) \times (m\pi)^2}{mn \left(\left(\frac{m}{A}\right)^2 + \left(\frac{n}{B}\right)^2\right)^2 \pi^6 DA^2} + \nu \times \frac{-\frac{\sin\left(\frac{m\pi x}{A}\right) \times 16q \sin\left(\frac{n\pi y}{B}\right) \times (n\pi)^2}{B}}{Bmn \left(\left(\frac{m}{A}\right)^2 + \left(\frac{n}{B}\right)^2\right)^2 \pi^6 D} \right)$$

$$M_y = -D \times \sum_{m=1}^{250} \sum_{n=1}^{250} \left(\nu \times \frac{\sin\left(\frac{n\pi y}{B}\right) \times (-16)q \sin\left(\frac{m\pi x}{A}\right) \times (m\pi)^2}{mn \left(\left(\frac{m}{A}\right)^2 + \left(\frac{n}{B}\right)^2\right)^2 \pi^6 DA^2} + \frac{-\frac{\sin\left(\frac{m\pi x}{A}\right) \times 16q \sin\left(\frac{n\pi y}{B}\right) \times (n\pi)^2}{B}}{Bmn \left(\left(\frac{m}{A}\right)^2 + \left(\frac{n}{B}\right)^2\right)^2 \pi^6 D} \right)$$

and

$$M_{xy} = -D \times (1 - \nu) \times \sum_{m=1}^{250} \sum_{n=1}^{250} \left(\frac{16q \cos\left(\frac{m\pi x}{A}\right) \times m\pi \cos\left(\frac{n\pi y}{B}\right) \times n\pi}{BAmn \left(\left(\frac{m}{A}\right)^2 + \left(\frac{n}{B}\right)^2\right)^2 \pi^6 D} \right)$$

and where D is the flexural rigidity of the plate ($D = \frac{Eh^3}{12(1-\nu^2)}$ with h the thickness of the plate), A is the length of the plate, B is the width of the plate and q is the uniformly distributed load applied on the plate. Let's just look at the solution in the center of the plate : x and y will then be taken equal to A/2 and B/2 respectively.

6.1.2 Simulation with ANSYS

The plate considered here is made of aluminium (E=70 GPa, $\nu = 0.3$ and density $\rho = 2700 \text{ kg/m}^3$) and has the following dimensions : length A=3.27 m, width B=1.519 m and thickness h=0.002 m. A UDL q of 1 kPa is applied on the plate, the simulation is then run in ANSYS with the elements SHELL181, SHELL281 and SHELL63. The SHELL63 element, unlike the other two, does not take into account the shear deformation. As the problem is symmetrical with two planes of symmetry, it is possible to model only a quarter of the plate without changing the results obtained. To do this, symmetric boundary conditions must be applied : the normal displacement of the left and the bottom edge are blocked but not the tangential displacement. The normal and tangential rotation of these edges must also be blocked. The results are shown in Figure 37.

For clarity, only the results for M_1 have been plotted but similar results are obtained for M_2 . It was not possible to simulate a larger number of elements than those presented here because the student version of ANSYS is limited in the number of elements.

The graphs show the percentage error between the simulated moment M_1 and the theoretical moment in the center of the plate versus the number of elements per edge. The percentage error is

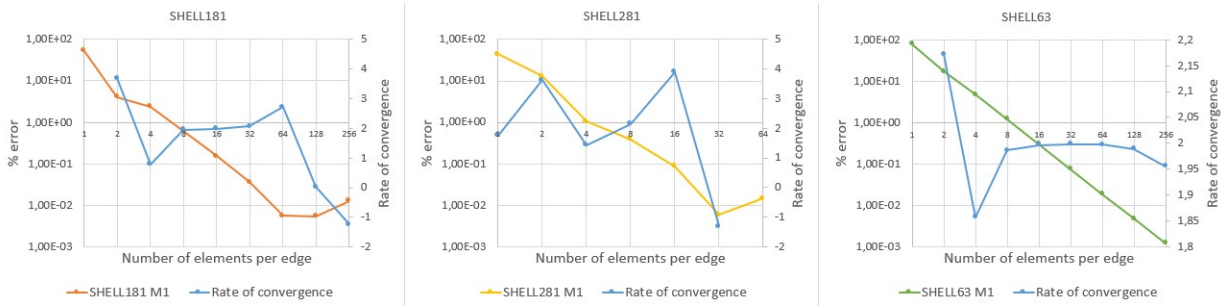


FIGURE 37: Percentage error and rate of convergence versus number of elements per edge for three different shell elements in ANSYS

calculated according to the formula : $\%error = \frac{M_{simulated} - M_{theoretical}}{M_{theoretical}} \times 100$.

The rate of convergence is also plotted on the figure. Let's call $M_e|m$ the percentage error calculated for the number of elements 2^m . The rate of convergence q is then given by the formula :

$$q = \frac{\log(M_e|m+1/M_e|m)}{\log(1/2)}.$$

As seen on the graph, the error is less than 1% for a number of elements greater than around 8 for SHELL181 and greater than 4 for SHELL281. However, the convergence is very poor for these elements as the percentage error starts to increase when the number of elements exceeds a certain value (beyond 64 elements for SHELL181 and beyond 32 elements for SHELL281). On the other hand for the element SHELL63, there seems to be a good convergence as the percentage error always decreases as the number of elements increases. It takes around 8 elements per edge to get a percentage error below 1% with this element.

Furthermore, for all three elements, the rate of convergence does not seem to converge to a value, as it is supposed to do normally. It is a bit better for the element SHELL63, whose rate of convergence seems to remain around 2.

6.1.3 Closure

In this short study, it was seen that the elements SHELL181 and SHELL281 do not seem to be very good for modelling a simply supported rectangular plate under UDL. Even if the convergence is quite fast, the percentage error increases again beyond a certain number of elements, which is not normal. Being restricted by the student version of ANSYS, it was not possible to see how the convergence is for a larger number of elements. But it is likely that the percentage error continues to increase for a larger number of elements and it may even exceed 1%.

On the other hand, the element SHELL63 seems to be a rather good choice for modelling this case, but this element is not in the default settings of ANSYS. Given these worrying results, one may wonder whether the software can really be trusted. Knowing this, extra care should be taken for futur projects using these elements.

In the following, the element SHELL281 will be used. Indeed, even if it is not ideal, the convergence is nevertheless satisfactory because the error is lower than 1%.

6.2 Balustrade

Let's now focus on the balustrade, which is made of corrugated plates. The aim will be to verify that the balustrade, the model of which has been provided by ESK Balustrade systems limited, complies with the European construction standards, Eurocode 9.

6.2.1 Model of the balustrade

The balustrade is made of 1050 aluminium sheet of Young's modulus $E=70$ GPa, of Poisson's ratio $\nu = 0.3$ and of density $\rho = 2700$ kg/m³. The yield stress S_y can be as low as 85 MPa for this material. Let's use this minimum value for future calculations to have a safety margin.

The balustrade is 2.998 m long, 1.500 m wide and 0.002 m thick. To comply with the SLS condition, the European standard says that it must be able to withstand a UDL of 1 kPa or a point load of 125 N. It should be checked that the maximum displacement is less than 25 mm and that the maximum stress does not exceed the yield stress of 85 MPa.

As the balustrade is doubly symmetrical, it is possible to model only a quarter of it in ANSYS. The point load applied will then be a quarter of 125 N. The study will be done with SHELL281, with 32 elements per edge, and the large displacement option will be switch on.

6.2.2 Modelling with ANSYS

The simulation was first carried out on a simple model of a flat plate to get an idea of the results obtained. with the same dimensions as seen above. The simulation was then run with the real model with the corrugated plates, and the results for both models are shown in the table below.

	Area load		Point load	
	Deflection max (m)	Utilisation	Deflection max (m)	Utilisation
Flat plate	0.054393	1.90392	0.018513	0.310205
Corrugated plate	0.014873	0.271188	0.00288	0.362094

The utilisation is calculated by dividing the maximum moment by the yield moment M_y , where the yield moment is given by $M_y = S_y \times t^2/6$ with t the thickness. The utility should be less than 1 for the SLS condition to be met. The von Mises criterion was used here for the calculation. As seen in the table, the SLS condition is not fulfilled for the flat plate with the area load, as the deflection exceeds 25 mm, and the utilisation exceeds 1. However, the corrugations make the plate stiffer which allows the plate to meet the SLS condition. For the point load, both plates meet the SLS condition, even though the corrugated plate deforms less than the flat plate. The model provided by the company therefore appears to comply with European standards for the SLS condition.

6.2.3 Boundary conditions

A criterion to be considered in designing the balustrade is the choice of the boundary conditions. Indeed, the plates in the simulation above are simply supported, but they can also be clamped, with no pull in and clamped with no pull in. The study below was conducted to see the influence of the different boundary conditions. It was done on the flat plate and on the corrugated plate, with the point load and the area load.

For a plate, the normal displacement on each side must be blocked to have a simply supported plate. In order to have a clamped plate, the plate must be simply supported and in addition the rotation parallel to the normal direction sides and the rotation parallel to the tangential direction sides must be blocked. To stop pull in, the plate must be simply supported and in addition the translation normal to the normal direction sides and the translation normal to the tangential direction sides must be blocked. The results are shown in Figure 38.

As seen on the graphs, the clamped and no pull in boundary conditions allows to have the lowest deflection for the same load applied. This should therefore be taken into account in the design of balustrades and plates in general, so that the deflection is as small as possible.

As the first simulation was done with a simply supported plate, it seems that choosing another

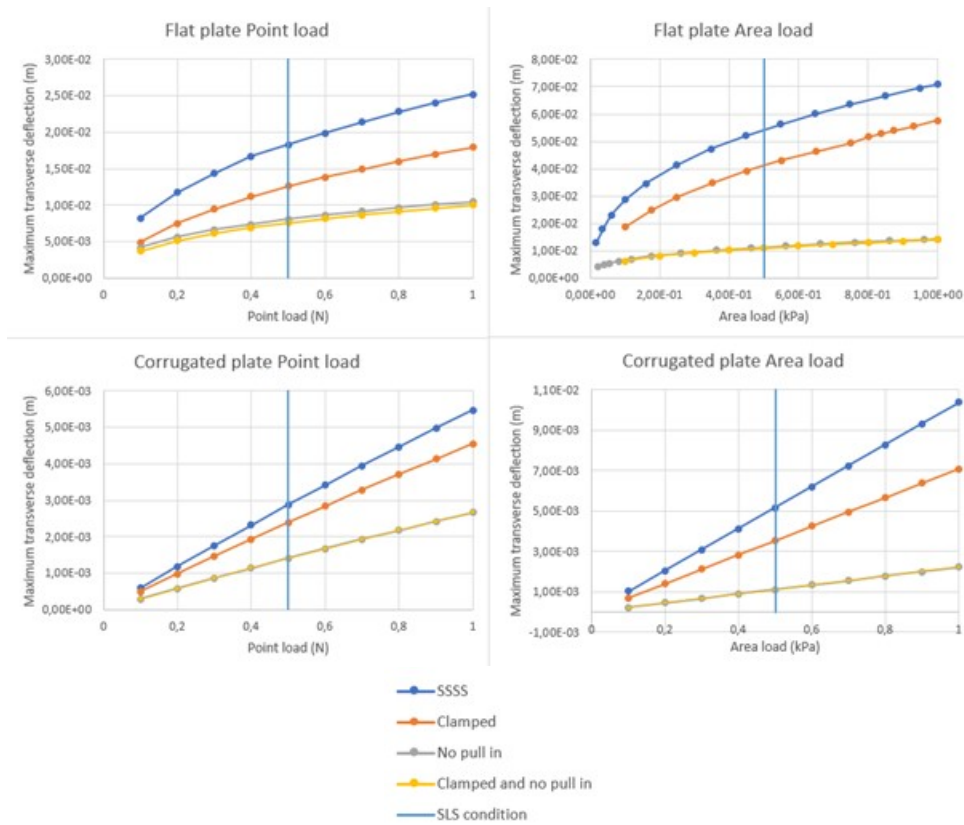


FIGURE 38: Maximum transverse deflection of plates with different boundary conditions

boundary condition will necessarily reduce the deflection of the balustrade. Thus, the European standards will still be met by this balustrade design. However, the report could not be finished before the internship ended.

7 Conclusion

During the three months of my internship, I was able to carry out five different projects which all taught me a lot.

With the beam project, I learned to verify the results given by ANSYS knowing the theoretical solution. I was also able to make a comparative study of the beam elements in ANSYS, to see which is the best choice depending on the applied load.

With the project of the plate with a hole, I was able to see the error of a bad mesh compared to a

good one, and thus understand the interest of spending time on the mesh during a modeling.

For the third study on the cylinder, the most interesting thing was to see that the elements used by ANSYS are not necessarily optimal in all situations. Indeed, Angus Ramsay has developed a new element, the Lamé Finite Element, which gives much more satisfactory results than those of ANSYS for the cylinder. It was very interesting to question what all engineers use, and not just apply what is already provided to us.

For the penultimate study on rotors, it was by reproducing some examples from a book that I was able to find an error in one of them. This taught me that errors are not impossible even in published books, and that one should not trust blindly but rather check the results by oneself when possible.

Finally, the commercial project was the most interesting for me because it allowed me to work on a concrete case provided by real clients. Even if I could not complete this project, the things I learned from it were very enriching.

References

[1] W. D. Pilkey, Peterson's Stress Concentration Factors, 2nd ed., John Wiley & Sons, New York, 1997, p.256

[2] Angus Ramsay, A Lamé Finite Element for the Analysis and Design of Rotating Discs, Ramsay Maunder Associates

[3] Hearn, E. J., Mechanics of Materials, Volume 1, Chapter 10, 3rd Edition, Butterworth-Heinemann, (2000)

[4] Angus Ramsay, Safe and Economical Simulation for the Built Environment, Ramsay Maunder Associates

[5] Vincenzo Vullo and Francesco Vivio, Rotors : Stress Analysis and Design, Springer-Verlag Italia 2013, Chapter 2

[6] Angus Ramsay, Navier Solution for the Simply Supported Rectangular Plate under UDL, Ramsay Maunder Associates

[7] S. Timoshenko, Theory of Plates and Shells, McGraw-Hill Book Company, 1959, Chapter 5